ornl

OAK RIDGE NATIONAL LABORATORY

UNION CARBIDE

OPERATED BY
UNION CARBIDE CORPORATION
FOR THE UNITED STATES
DEPARTMENT OF ENERGY

NUREG/CR-1477
ORNL/NUREG/TM-393

Heavy-Section Steel Technology Program Quarterly Progress Report for January-March 1980

G. D. Whitman R. H. Bryan

Prepared for the U.S. Nuclear Regulatory Commission
Office of Nuclear Regulatory Research
Under Interagency Agreements DOE 40-551-75 and 40-552-75

Printed in the United States of America. Available from
National Technical Information Service
U.S. Department of Commerce
5285 Port Royal Road, Springfield, Virginia 22161

Available from

GPO Sales Program
Division of Technical Information and Document Control
U.S. Nuclear Regulatory Commission
Washington, D.C. 20555

NUREG/CR-1477
ORNL/NUREG/TM-393
Dist. Category RF

Contract No. W-7405-eng-26

Engineering Technology Division

HEAVY-SECTION STEEL TECHNOLOGY PROGRAM QUARTERLY PROGRESS REPORT FOR JANUARY–MARCH 1980

G. D. Whitman R. H. Bryan

Manuscript Completed – June 9, 1980
Date Published – July 1980

Prepared for the
U.S. Nuclear Regulatory Commission
Office of Nuclear Regulatory Research
Under Interagency Agreements DOE 40-551-75 and 40-552-75

NRC FIN No. B0119

Prepared by the
OAK RIDGE NATIONAL LABORATORY
Oak Ridge, Tennessee 37830
operated by
UNION CARBIDE CORPORATION
for the
DEPARTMENT OF ENERGY

CONTENTS

PREFACE

The Heavy-Section Steel Technology (HSST) Program, which is sponsored by the Nuclear Regulatory Commission, is an engineering research activity devoted to extending and developing the technology for assessing the margin of safety against fracture of the thick-walled steel pressure vessels used in light-water-cooled nuclear power reactors. The program is being carried out in close cooperation with the nuclear power industry. This report covers HSST work performed in January through March 1980, except for subcontractor contributions which may cover the three-month period ending in February. The work performed by Oak Ridge National Laboratory (ORNL) and by subcontractors is managed by the Engineering Technology Division. Major tasks at ORNL are carried out by the Engineering Technology Division and the Metals and Ceramics Division. Prior progress reports on this program are ORNL-4176, ORNL-4315, ORNL-4377, ORNL-4463, ORNL-4512, ORNL-4590, ORNL-4653, ORNL-4681, ORNL-4764, ORNL-4816, ORNL-4855, ORNL-4918, ORNL-4971, ORNL/TM-4655 (Vol. II), ORNL/TM-4729 (Vol. II), ORNL/TM-4805 (Vol. II), ORNL/TM-4914 (Vol. II), ORNL/TM-5021 (Vol. II), ORNL/TM-5170, ORNL/NUREG/TM-3, ORNL/NUREG/TM-28, ORNL/NUREG/TM-49, ORNL/NUREG/TM-64, ORNL/NUREG/TM-94, ORNL/NUREG/TM-120, ORNL/NUREG/TM-147, ORNL/NUREG/TM-166, ORNL/NUREG/TM-194, ORNL/NUREG/TM-209, ORNL/NUREG/TM-239, NUREG/CR-0476 (ORNL/NUREG/TM-275), NUREG/CR-0656 (ORNL/NUREG/TM-298), NUREG/CR-0818 (ORNL/NUREG/TM-324), NUREG/CR-0980 (ORNL/NUREG/TM-347), NUREG/CR-1197 (ORNL/NUREG/TM-370), and NUREG/CR-1305 (ORNL/NUREG/TM-380).

SUMMARY*

1. PROGRAM ADMINISTRATION AND PROCUREMENT

The Heavy-Section Steel Technology (HSST) Program is an engineering research activity conducted by the Oak Ridge National Laboratory (ORNL) for the Nuclear Regulatory Commission (NRC) in coordination with other research sponsored by the federal government and private organizations. The program comprises studies related to all areas of the technology of materials fabricated into thick-section primary-coolant containment systems of light-water-cooled nuclear power reactors. The principal area of investigation is the behavior and structural integrity of steel pressure vessels containing cracklike flaws. Current work is organized into the following tasks: (1) program administration and procurement, (2) fracture mechanics analyses and investigations, (3) investigations of irradiated materials, (4) thermal shock investigations, and (5) pressure vessel investigations.

The work performed under the existing research and development subcontracts is included in this report.

Eleven program briefings, reviews, or presentations were made during the quarter.

2. FRACTURE MECHANICS ANALYSES AND INVESTIGATIONS

A combined pressure-thermal loading stress analysis of a boiling-water reactor feedwater nozzle has been made with ADINA and ADINAT codes to provide input to the BIGIF program. Calculations of stress-intensity factors K_I made by BIGIF for combined and pressure-only loadings were made for nozzle-corner cracks of various depth. A transient heat transfer calculation for a thermal shock to an intermediate test vessel nozzle corner was made with the ADINAT code for use in investigating pressurized thermal shock.

---

*Conversions from SI to English units for all SI quantities are listed on a foldout page at the end of this report.

Data and fracture surfaces from tests of fracture toughness specimens are being studied to develop a mechanistic model of the ductile-cleavage transition. Several photoelastic models have been tested to investigate damping in dynamic fracture; preliminary conclusions are that stress wave attenuation is not a major contributor to energy loss but late-breaking ligaments are. Photoelastic materials have been prepared for investigating the importance of higher-order terms in specimen analysis.

3. INVESTIGATIONS OF IRRADIATED MATERIALS

Impact testing of Charpy V-notch specimens from the Third HSST Irradiation Series was started after testing and calibration of the hot-cell equipment were completed.

Irradiation of the first capsule in the Fourth HSST Irradiation Series continued with excellent temperature control. Dosimetry results from the experiment with a dummy capsule and thermal shield were analyzed for the first capsule position; and a similar experiment was prepared for the second capsule, which is being assembled.

4. THERMAL SHOCK INVESTIGATIONS

Additional posttest analyses of thermal shock experiment TSE-5 produced corrected values of estimated crack depths and crack velocity. Data concerning K_{Ic} and K_{Ia} were evaluated further, a 3-D finite-element calculation of K_I for the final crack shape was made, and 2-D calculations were checked by an independent method of analysis.

A series of design calculations for the next thermal shock experiment, TSE-5A, was performed to clarify the ranges of parameters that would lead to an acceptable experiment.

5. PRESSURE VESSEL INVESTIGATIONS

Development of a seam-welding process that could be used to produce a low-upper-shelf weld (Charpy energy $\lesssim$68 J) in intermediate test vessel

V-8A is being initiated by subcontract. If the development phase is successful, this special process will be used on the vessel and on a prolongation which will be used for characterizing the material.

Further plans and cost estimates were made in support of NRC's work on acoustic emission (AE) at the Pacific Northwest Laboratory. Intermediate test vessel V-7 and flawed cylindrical sections that could be welded into another vessel were considered as alternative objects of AE tests.

HEAVY-SECTION STEEL TECHNOLOGY PROGRAM QUARTERLY PROGRESS REPORT FOR JANUARY–MARCH 1980

G. D. Whitman R. H. Bryan

ABSTRACT

The Heavy-Section Steel Technology Program is an engineering research activity conducted by the Oak Ridge National Laboratory for the Nuclear Regulatory Commission. The program comprises studies related to all areas of the technology of materials fabricated into thick-section primary-coolant containment systems of light-water-cooled nuclear power reactors. The investigation focuses on the behavior and structural integrity of steel pressure vessels containing cracklike flaws. Current work is organized into five tasks: (1) program administration and procurement, (2) fracture mechanics analyses and investigations, (3) investigations of irradiated materials, (4) thermal shock investigations, and (5) pressure vessel investigations.

Nozzle-corner cracks under combined pressure and thermal loadings are being analyzed. Photoelastic tests and finite-element computations were conducted to study the mechanisms of damping in crack propagation. Irradiation of the first specimens in the Fourth HSST Irradiation Series continued. Additional posttest analyses of the last thermal shock experiment included 3-D finite-element calculations, and further material studies and analyses were performed for the next experiment. Contract details were completed for preparation of a low-upper-shelf seam weld in intermediate test vessel V-8A.

---

1. PROGRAM ADMINISTRATION AND PROCUREMENT

G. D. Whitman

The Heavy-Section Steel Technology (HSST) Program, a major safety program sponsored by the Nuclear Regulatory Commission (NRC), is concerned with the structural integrity of the primary systems (particularly the reactor pressure vessels) of light-water-cooled nuclear power reactors. The structural integrity of these vessels is ensured by (1) designing and fabricating them according to the standards set by the code for nuclear pressure vessels, (2) detecting flaws of significant size that occur durin fabrication and in service, and (3) developing methods of producing quantitative estimates of conditions under which fracture could

occur. The program is concerned mainly with developing pertinent fracture technology, including knowledge of the material used in these thick-walled vessels, the flaw growth rate, and the combination of flaw size and load that would cause fracture and thus limit the life and/or operating conditions of this type of reactor plant.

The program is coordinated with other government agencies and with the manufacturing and utility sectors of the nuclear power industry in the United States and abroad. The overall objective is quantification of safety assessments for regulatory agencies, for professional code-writing bodies, and for the nuclear power industry. Several activities are conducted under subcontracts by research facilities in the United States and through informal cooperative efforts on an international basis. Two research and development subcontracts are currently in force.

Administratively, the program is organized into five tasks, as reflected in this report: (1) program administration and procurement, (2) fracture mechanics analyses and investigations, (3) investigations of irradiated material, (4) thermal shock investigations, and (5) pressure vessel investigations.

Two sections of HSST Plate 03 designated for the International Atomic Energy Agency Cooperative Irradiation Program were sent to Germany for preparation of specimens for the Comision National de Energia Atomica of Argentina.

Thirty-six pieces of HSST Plate 07 were shipped to Materials Research Laboratory for use in the crack-arrest test round robin.

During this quarter, 11 program briefings, reviews, or presentations were made by the HSST staff at technical meetings and at program reviews for the NRC staff or visitors.

2. FRACTURE MECHANICS ANALYSES AND INVESTIGATIONS*

2.1 Determination of K-Factors for Nozzle-Corner Flaws Under Combined Pressure-Thermal Loading

J. W. Bryson B. R. Bass
J. B. Drake

Work continues on determining K_I distributions for quarter-circular-shaped nozzle-corner flaws under combined internal pressure-thermal loading. The BIGIF code is being used in conjunction with MULT-NOZ, ADINAT, and ADINA finite-element codes in performing this work. The steady-state temperature distribution reported last quarter,[1] which simulates normal operating conditions of a boiling-water reactor (BWR), was input to ADINA, and a complete thermoelastic solution was obtained. The resulting uncracked normal stress distribution was then input to BIGIF, and stress intensity factor K_I distributions were obtained for four different sizes of nozzle-corner flaws (a/T = 0.14, 0.29, 0.53 and 0.81), where a = crack depth and T = thickness across nozzle corner. Comparisons of K values for the combined pressure-thermal loading with those for the same internal pressure loading (6.9 MPa) acting alone are shown in Figs. 2.1 through 2.4. Maximum values of K_I were obtained near the free surface of the nozzle for combined pressure-thermal loading; these values were 20 to 40% higher than the corresponding values resulting from internal pressure acting alone.

Pressurized thermal shock studies are also being conducted using an intermediate test vessel (ITV) configuration (see Fig. 2.5) that has a relatively thicker vessel and larger nozzle than does the BWR configuration. Work is under way to obtain a fully transient solution for the pressure-thermal environment depicted in Fig. 2.5. In this problem the system is initially at T = 290°C, and the nozzle fluid then undergoes a step change in temperature from T = 290°C to T = 5°C. The ADINAT code is being used to perform the heat flow analysis, and ADINA and BIGIF will then be used to calculate stress and K_I distributions for selected time intervals into the transient. Figures 2.6 through 2.10 show representative

*Conversions from SI to English units for all SI quantities are listed on a foldout page at the end of this report.

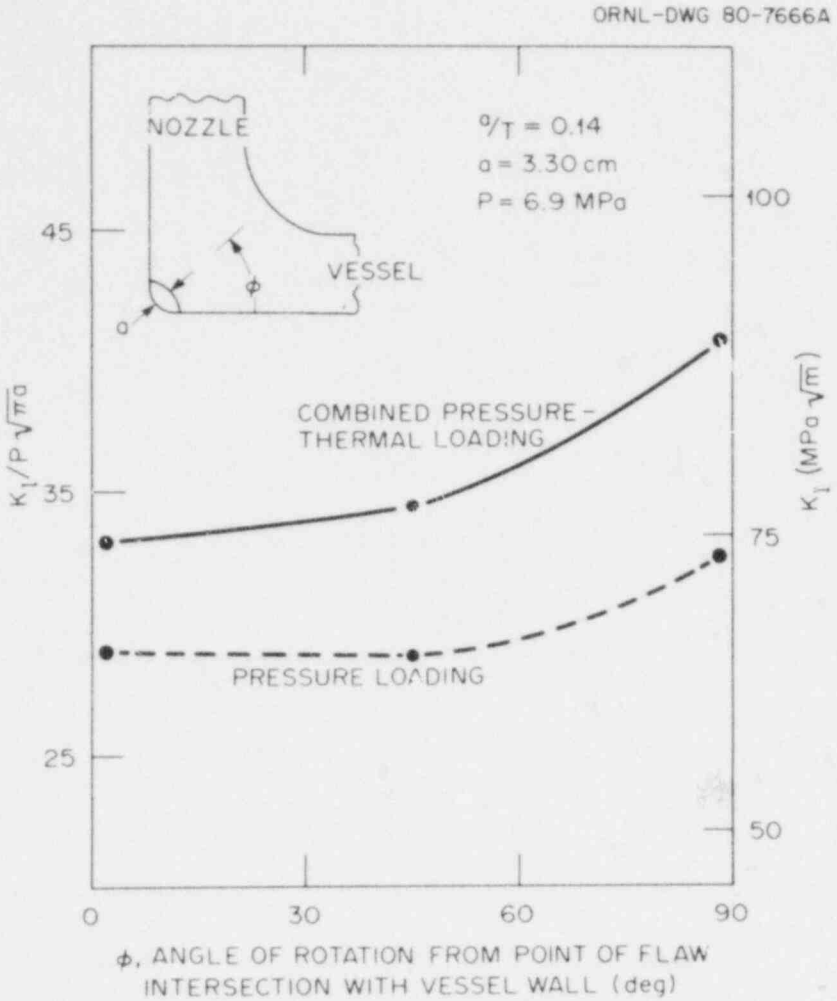

Fig. 2.1. K_I distributions for BWR nozzle corner flaw (a/T = 0.14) under combined pressure-thermal loading (steady-state) and under pressure loading acting alone.

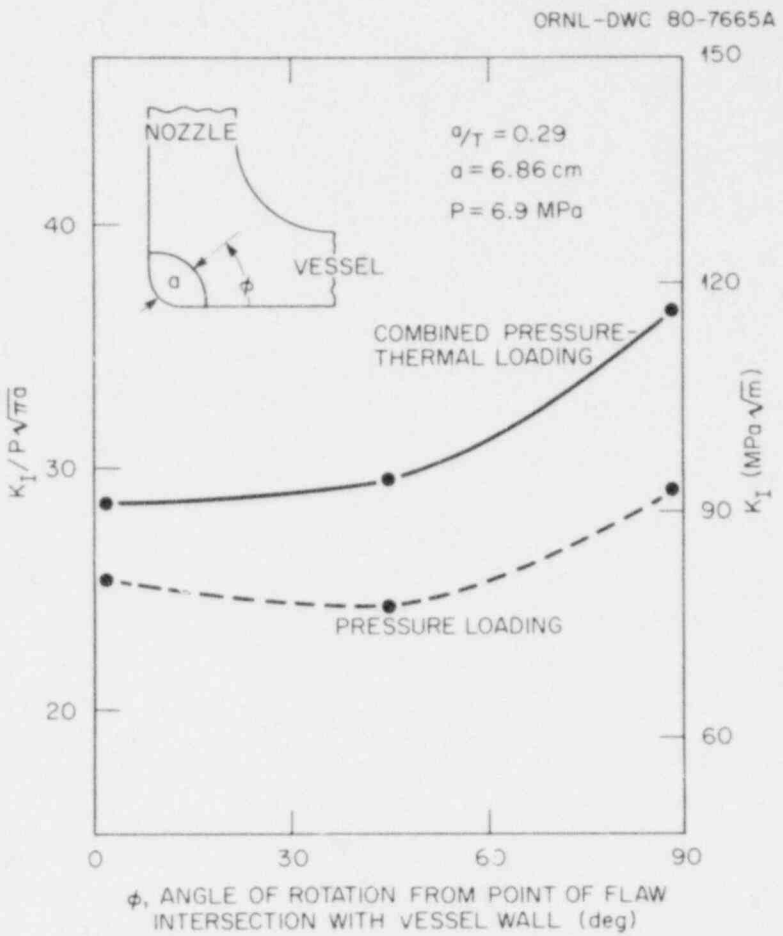

Fig. 2.2. K_I distributions for BWR nozzle corner flaw (a/T = 0.29) under combined pressure-thermal loading (steady-state) and under pressure loading acting alone.

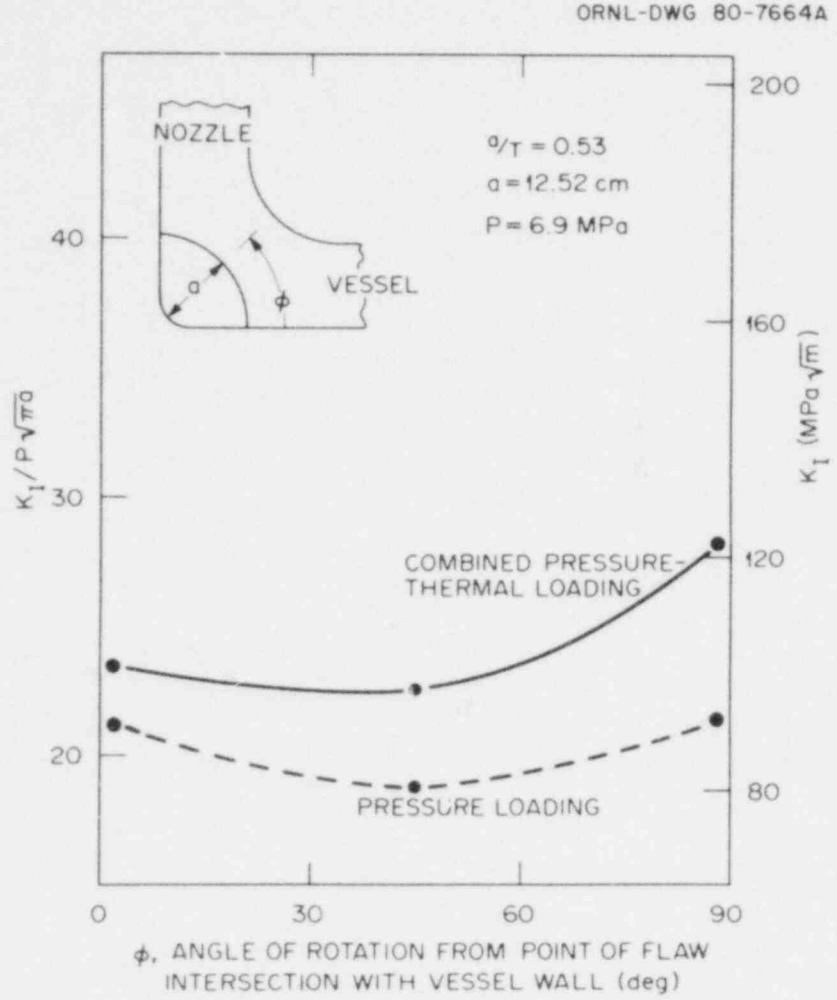

Fig. 2.3. K_I distributions for BWR nozzle corner flaw (a/T = 0.53) under combined pressure-thermal loading (steady-state) and under pressure loading acting alone.

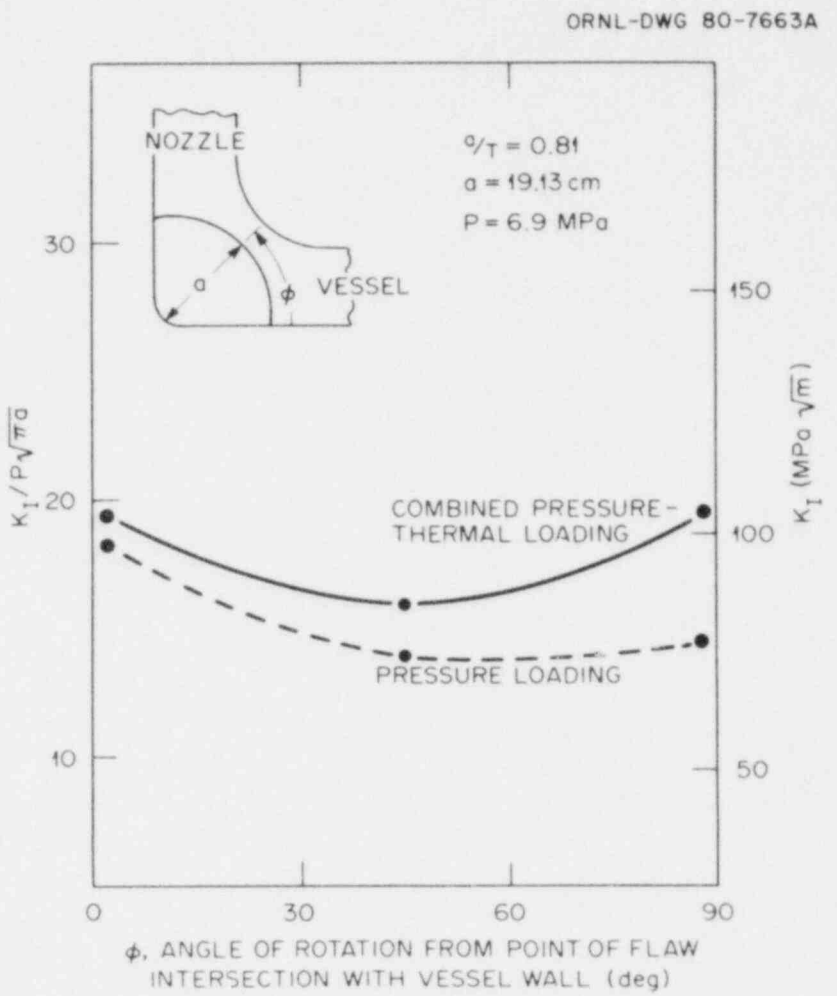

Fig. 2.4. K_I distributions for BWR nozzle corner flaw (a/T = 0.81) under combined pressure-thermal loading (steady-state) and under pressure loading acting alone.

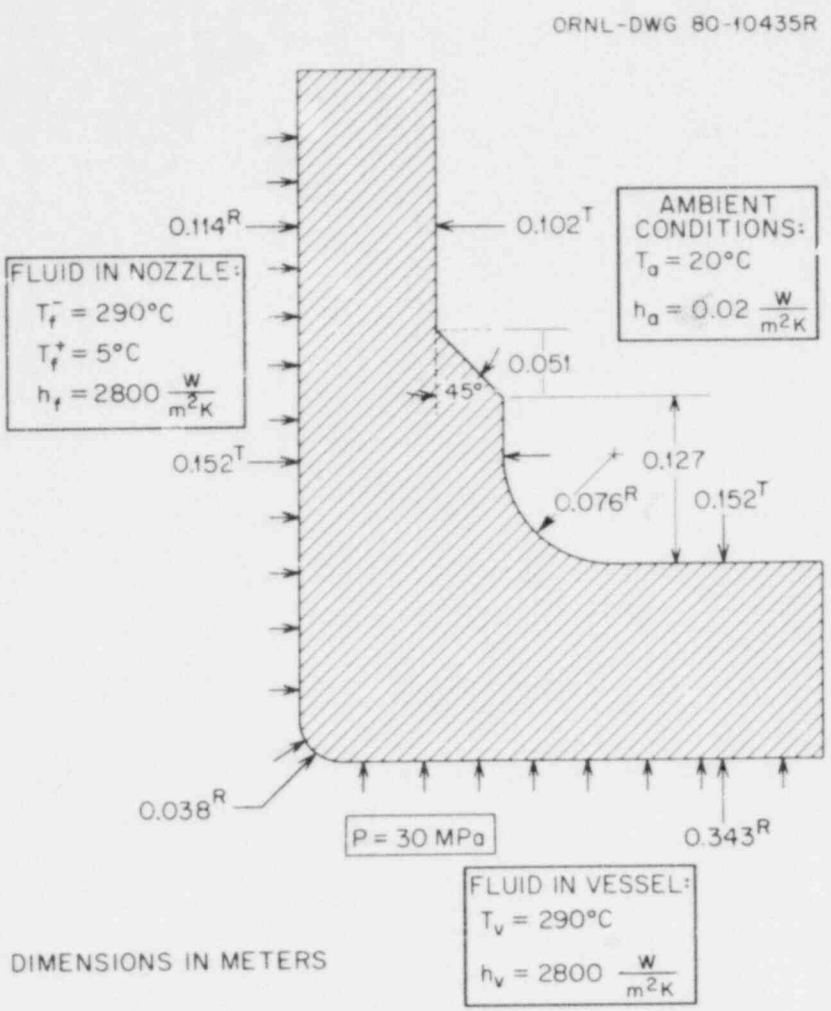

Fig. 2.5. Longitudinal section of an intermediate test vessel with pressurized thermal shock analysis parameters.

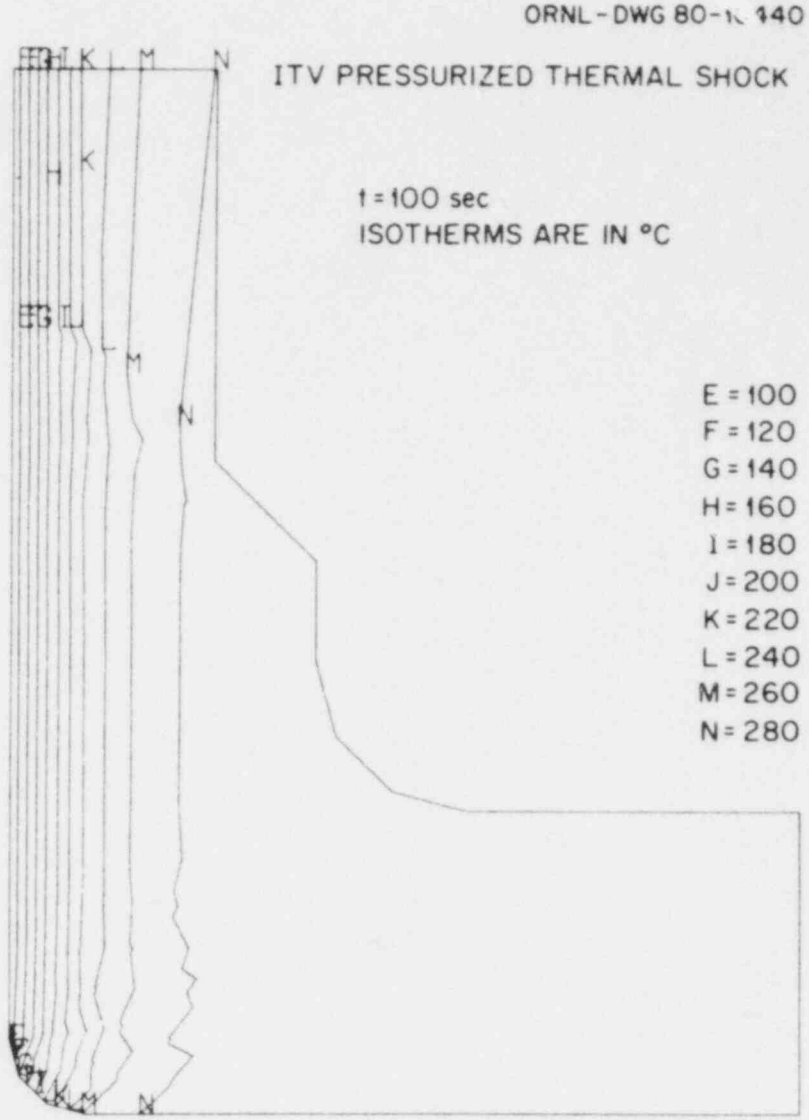

Fig. 2.6. Temperature distribution at t = 100 s for ITV subjected to pressurized thermal shock (see Fig. 2.5).

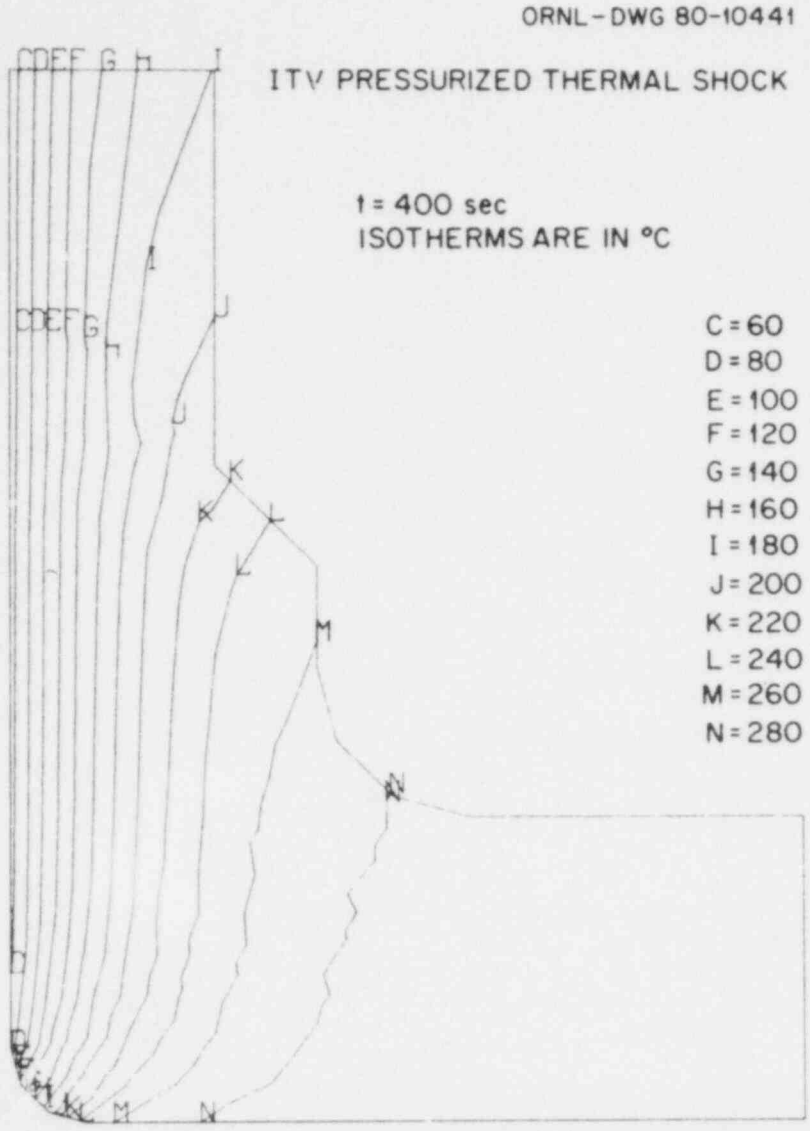

Fig. 2.7. Temperature distribution at t = 400 s for ITV subjected to pressurized thermal shock (see Fig. 2.5).

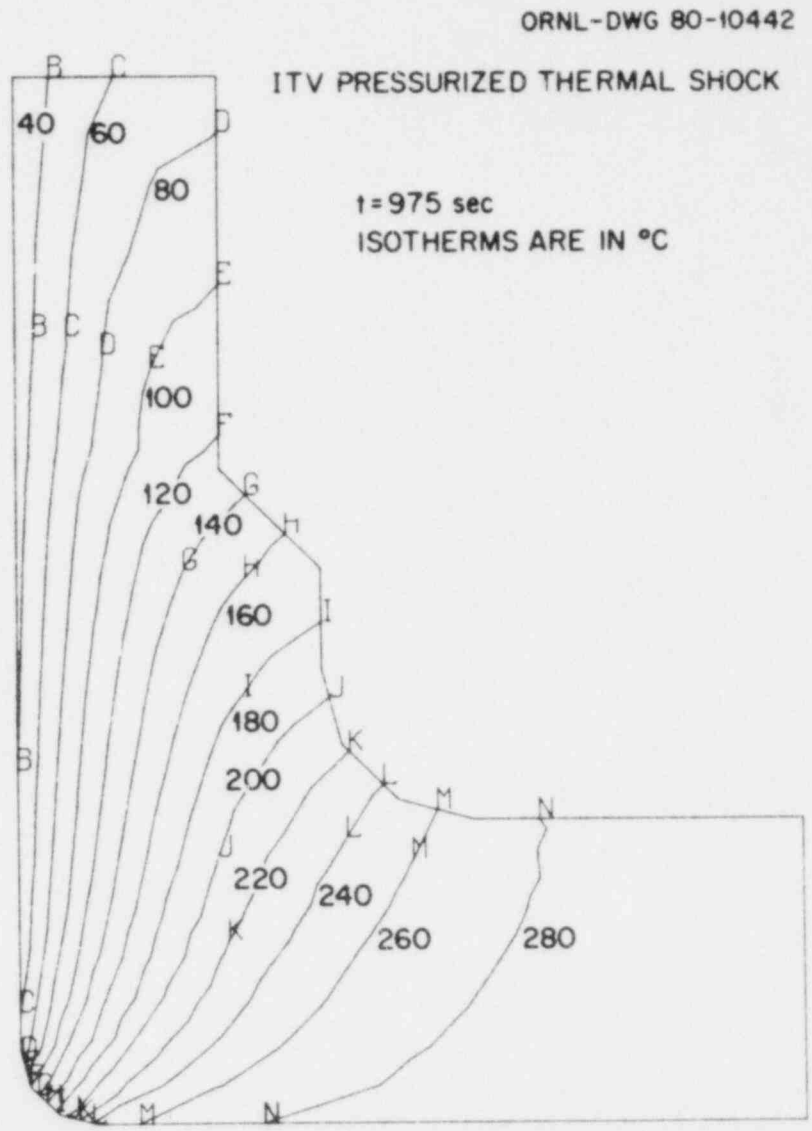

Fig. 2.8. Temperature distribution at t = 975 s for ITV subjected to pressurized thermal shock (see Fig. 2.5).

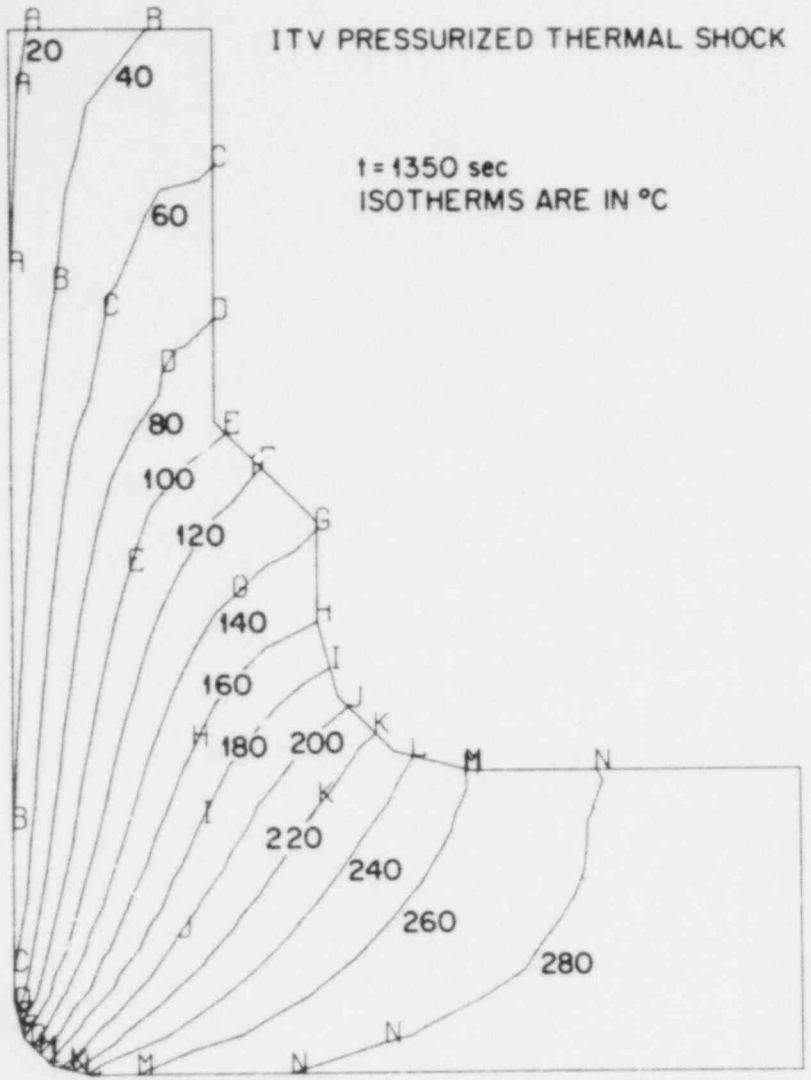

Fig. 2.9. Temperature distribution at t = 1350 s for ITV subjected to pressurized thermal shock (see Fig. 2.5).

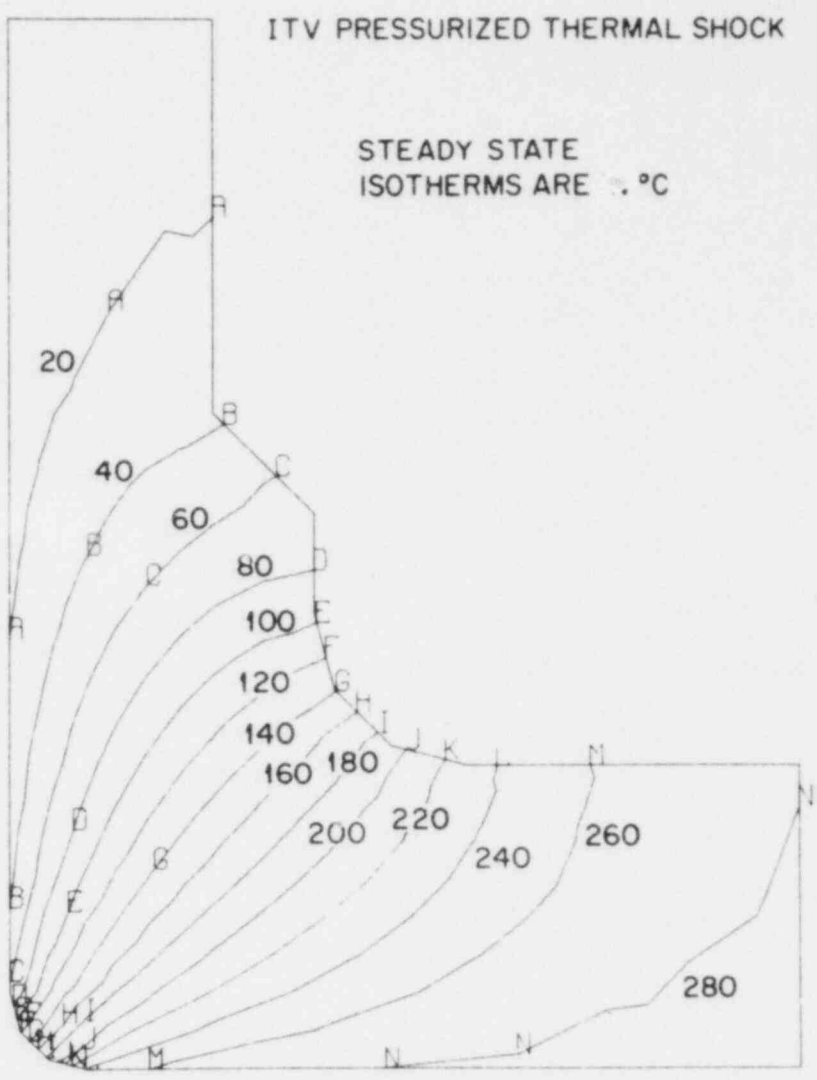

Fig. 2.10. Temperature distribution at steady state for ITV subjected to pressurized thermal shock (see Fig. 2.5).

temperature distributions calculated by ADINAT for this prescribed pressure-thermal loading.

2.2 Investigation of Damping and of Cleavage-Fibrous Transition in Reactor Grade Steel*

W. L. Fourney†

2.2.1 Introduction

This research program is designed to investigate the effect of damping on fracture propagation as well as to study the transition region between cleavage and ductile fracture. A complete understanding of both of these phenomena is extremely important in predicting fast fracture behavior of a structure.

We were originally funded to conduct three separate tasks.

A. Examine the phenomenon of ductile-to-cleavage transition during fracture.

B. Examine more closely the effects of damping on the determination of K and propagation behavior.

C. Conduct dynamic 2-D finite-element computations to support findings in the preceding two tasks.

A fourth task (funded with a savings realized in overhead charges) was added — to examine further the effect of higher-order terms on the accuracy of stress intensity factor K determination. A particular concern in this task is the effect of specimen size and shape on these higher-order terms.

Five mechanisms for energy loss warrant examination.

1. Energy loss is associated with the rapid drop in K from high preinitiation K_Q values to a much lower dynamic value K_D.

2. Energy loss occurs whenever energy is changed in form; for example, in Homalite 100, the static modulus of elasticity is much lower than

---

*Work sponsored by HSST Program under UCCND Subcontract 7778 between Union Carbide Corporation Nuclear Division and the University of Maryland.

†Department of Mechanical Engineering, University of Maryland, College Park, MD 20742.

the dynamic one. Hence, when the energy (even potential energy) goes from a static-state value to a dynamic one, a loss occurs as a result of the change in elastic modulus E.

3. If late-breaking ligaments are present, as in a steel sample, energy can be lost in ligament formation. If the crack tends to close behind the running tip, energy may be lost because of rubbing or impingement of these ligaments.

4. Energy is lost because of the attenuation of stress waves.

5. Energy is lost in vibrations that are damped out after arrest occurs.

We feel the first three sources of damping are the most important, and we are concentrating our efforts along those lines. Tasks B and C will help us understand damping losses more clearly. We are using our computer code to analyze effects of late-breaking ligaments and strip-zone loadings on the stress intensity at the crack tip. In addition, we are running photoelastic experiments to determine the amount of damping in polymeric models and are investigating such factors as the effects of specimen size, specimen shape and thickness, K_Q level, and initial crack length on the loss of energy through damping.

Task A is designed to increase understanding of the brittle-to-ductile transition in fracturing. By conducting electron microprobe studies of fracture surfaces, we hope to develop a plausible model of the stress-strain conditions that control cleavage-fibrous fracturing. The ultimate aim of this task is to recommend a plan for developing adequate understanding of the transition region in relation to use of J-R curves.

The final task on higher-order terms that we added to our program will permit us to increase the accuracy of the K determination from our photoelastic data.

2.2.2 Progress to date

Task A: Brittle to Ductile Transition. Progress in the transition study is not so good as we had hoped. We had planned to have a preliminary mechanical model by this time that would be used to explain the transition region. We are, however, making progress, and the work needed

to formulate that model is under way. As indicated in the last progress report, we have managed to generate considerable interest in this topic at other research organizations. Landis (Westinghouse) and Andrews (General Electric) have just sent data which will permit us to study the scatter of toughness values obtained when fracturing begins with cleavage. Additional data may also be available from the Naval Research Laboratory (NRL), Naval Ship Research and Development Center (NSRDC) — Annapolis, and Del Research.

Studies are under way at Del Research and at NSRDC to investigate fracture in the temperature range where fractures starting as slow, stable, fibrous tearing can be made to change to abrupt cleavage. This change is triggered by the development of an actual or near approach to a tearing instability. Del Research is using A36 steel samples and NSRDC, an A533B steel. The Del Research data and half of each specimen are now available to us. Specimens and data from NSRDC will be available in about a month.

These samples, when received, will be viewed under the scanning electron microscope (SEM) in the regions adjacent to the onset of cleavage. In particular, we would like to compare the tensile stretch of local regions of fibrous separation in the fibrous zone and in the cleavage zones. These SEM photomicrographs will then be compared with those obtained from samples tested at lower temperatures, and the influence of temperature on the size and ductile stretch of fibrous separations will provide valuable information for developing a mechanistic model.

Table B: Damping. Five different photoelastic test series have been conducted to investigate various aspects of damping.

1. Four experiments were completed to determine if face grooving of compact tension (CT) specimens increased the damping loss. If the stress wave attenuation were a major contributor to the loss of energy, then the face grooving would cause larger wave dispersion and losses should increase. Data from the experiments indicated no increased damping over ungrooved samples; thus, wave dispersion seems to account for only a small part of damping.

2. Fifteen models have been tested to determine the influence of unbroken ligaments on fracture. These ligaments were formed by bonding a

tough structural adhesive into pockets machined into the Homalite 100 CT specimens. Models with 2, 4, and 6 ligaments have been tested. Depending on the value of the initial K_Q and the cross-sectional area of the ligaments, the crack would either propagate through the ligament or arrest permanently. All results have not beeen analyzed, but initial indications are that the ligaments greatly increase energy loss in the specimens. The ligaments used were made of a material that was too tough, so some of these experiments will be repeated with a more brittle adhesive.

3. Four experiments have been conducted to study the influence of starter crack length (a_o) on the crack jump distance Δa. These were done to clarify earlier damping results that showed a high dependence of damping on initial crack length. Initial results indicate that for the same value of K_Q, smaller a_o gives longer Δa. Analysis of these data is incomplete in regard to damping because static calibration of the model geometry still needs to be accomplished.

4. Seven experiments were carried out with large CT specimens (one and one-half times as large as the standard size) to study the influence of specimen size on damping. Preliminary results (four out of seven tests analyzed) show that energy loss is dependent on specimen size.

5. Three tests have also been conducted with small CT specimens (three-fourths standard size), and results of these tests are still being analyzed.

Task C: 2-D Computations. Good progress has been made with the finite-element code (SAMCR), and crack propagation in plastic CT specimens is predicted quite well, with about a 20% overestimation of crack jump length. This 20% figure agrees with the percentage of energy lost in damping during fracture surface formation for the same configuration. Since the code includes no damping, the 20% overestimate is what would be expected.

Work is progressing on modifying the code to run a comparison with thermal shock experiment TSE-5 at ORNL. We had hoped to have some preliminary results on that comparison by now, but the necessary modifications in geometry and thermal loading are not yet complete.

Task D: Higher-Order Terms. The best method for investigating the effects of speciment size on higher-order terms appears to be stress-

freezing-3-D photoelastic analysis. A suitable material for this work has been procured, and calibration tests are being conducted to determine the proper stress-freezing temperature and the associated fringe constant. Calculations to determine the critical load required for different crack length growth in different sizes of modified compact tension (MCT) specimens have been completed. We should be able to determine the threshold value of K required for crack growth by the end of April, and we will then begin testing three sizes of MCT specimens. If time permits, this will be followed by testing of two other specimen geometries — possibly a notch-bend sample and one other.

Reference

1. J. W. Bryson et al., "Determination of K-Factors for Nozzle Corner Flaws Under Combined Pressure-Thermal Loading," *HSST Program Quart. Prog. Rep. October-December 1979*, ORNL/NUREG/TM-380, pp. 45-50.

3. INVESTIGATIONS OF IRRADIATED MATERIALS*

R. G. Berggren J. W. Woods
T. N. Jones D. A. Canonico

3.1 Third 4T-CTS Irradiation Study

The calibration of our in-cell Charpy impact test machine was checked, and testing of the Charpy V-notch impact specimens is now in progress. Impact testing of unirradiated control specimens was conducted on both our out-of-cell and in-cell impact test machines to obtain baseline data before conducting tests on irradiated specimens. The initial tests were conducted on specimens with irradiation temperatures[1] farthest from the target irradiation temperature (288°C). Sufficient data to justify reporting results have not been accumulated, but the Charpy impact test program should be completed in the next quarter.

3.2 Fourth HSST Irradiation Series

Irradiation of the first capsule of this series[1] continued through this quarter Temperature control continues to be excellent, with variations close to those previously reported.[2]

The neutron dosimetry experiment being prepared last quarter[2] was conducted with a dummy capsule in the irradiation capsule position and the thermal shield in place. Analysis of these dosimetry results shows fast neutron fluxes of 1.5 to 1.9 × 10^{12} neutrons/(cm^2·s) (E > 1 MeV) for 75% of the specimen crack fronts (points of interest in testing). Fluxes for other specimens range downward from 1.5 × 10^{12} neutrons/(cm^2·s) (E > 1 MeV) to about 0.6 × 10^{12} neutrons/(cm^2·s) (E > 1 MeV). Final values for fast neutron fluxes and fluences will be determined by analysis of dosimeters included in the specimen capsule.

The thermal shield for the second capsule in this irradiation series is being prepared, and a neutron dosimetry experiment is being readied for

---

*Conversions from SI to English units for all SI quantities are listed on a foldout page at the end of this report.

operation in this second bulk shielding reactor (BSR) capsule position. Assembly of the second capsule is in progress.

References

1. R. G. Berggren et al., "Toughness Investigations of Irradiated Materials," *Heavy-Section Steel Technology Program Quart. Prog. Rep. July–September 1979*, ORNL/NUREG/TM-370, pp. 27–39.

2. R. G. Berggren et al., "Toughness Investigations of Irradiated Materials," *Heavy-Section Steel Technology Program Quart. Prog. Rep. October–December 1979*, ORNL/NUREG/TM-380, pp. 60–61.

4. THERMAL SHOCK INVESTIGATIONS*

R. D. Cheverton S. E. Bolt
S. K. Iskander D. G. Ball
R. S. Wallace

4.1 Introduction

During this report period for the Thermal Shock Program, the posttest analysis of TSE-5 was continued, material used for the TSE-5 test cylinder and material under consideration for a future experiment were further characterized, and calculations pertaining to the next thermal shock experiment (TSE-5A) were performed. Previous discussions of this subject matter are found in Refs. 1 and 2.

4.2 Posttest Analysis of TSE-5

4.2.1 Estimate of crack depth from crack-opening displacements (COD) data

The COD measurements made with Ailtech strain gages at the inner surface of the TSE-5 test cylinder can be used to obtain estimates of crack depth by calculating the relation between COD and crack depth. This relation was obtained from the 2-D fracture mechanics analysis of TSE-5, and the results are shown in Fig. 4.1 for times corresponding to the three initiation-arrest events. The COD-gage output was converted to actual COD by calibrating typical COD gages in an MTS machine.[2] The calibration factor COD/ϵ was (1) constant over the full range of the gage, (2) essentially independent of the temperature range of interest (93 to −196°C), and (3) equal to 25 mm.

Fractional crack depths (a/w) as derived from the COD data and as measured directly are presented in Table 4.1. The COD values used were the averages of COD gages 5 and 7 (central portion of cylinder).[1]

The differences observed in Table 4.1 are probably within the accuracy of the measurements and calculations. However, the general trend of the differences is consistent with the 3-D effect that developed as

*Conversions from SI to English units for all SI quantities are listed on a foldout page at the end of this report.

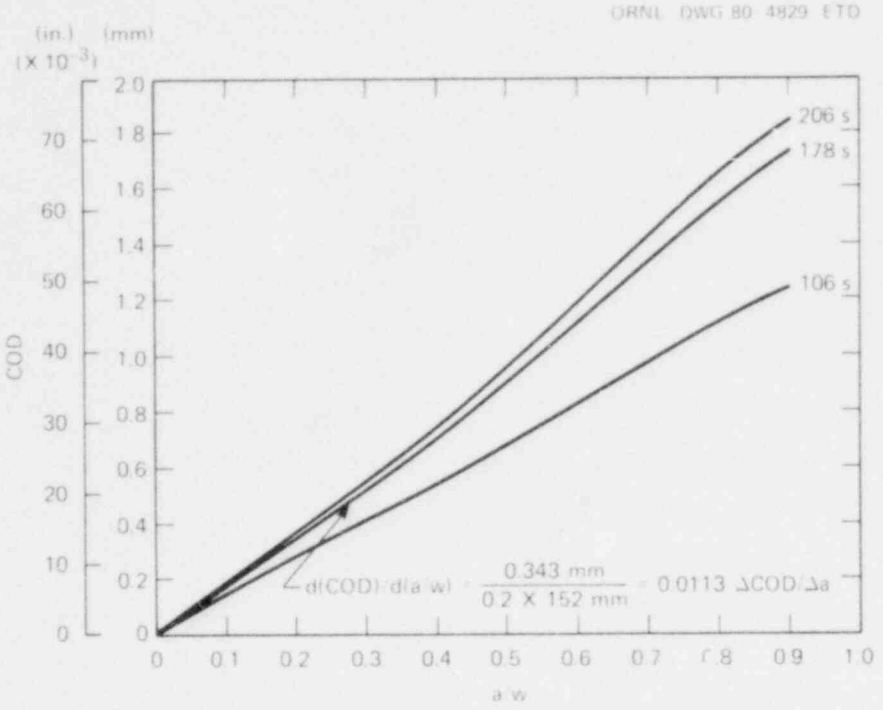

Fig. 4.1. Calculated COD vs a/w for TSE-5.

Table 4.1. Crack depth as derived from COD data and as measured directly

Time (s)	Fractional crack depth (a/w)	
	Direct	From COD
106	0.10[a]	0.12
106	0.23[a]	0.21
178	0.23[a]	0.22
178	0.63[b]	0.55
206	0.63[b]	0.55
206	0.80[a]	0.72

[a]Fracture surface measurement.

[b]Ultrasonic test measurement.

the flaw propagated deeper into the wall, increasing the nonuniformity in crack depth (which was shallower near the ends). The nonuniformity tends to decrease the COD for a given crack depth, and this effect is not included in the 2-D analysis. Thus, a 3-D analysis would increase the a/w values derived from the COD measurements above those shown in Table 4.1; the effect increases with increasing crack depth. A 3-D analysis is in progress.

4.2.2 Crack velocity measurements

An attempt was made to determine crack velocity during TSE-5 by measuring the crack-opening rate at the surface of the test cylinder with two of nine COD gages. Data from the two gages, which were located near midlength of the test cylinder, were recorded on fast-phenomena recorders. The effort was developmental and was prompted by future plans for a long-crack-jump experiment.

Because of difficulties encountered with the fast recorders during TSE-5, only the second of the three crack jumps was recorded properly. The COD vs time for this event is shown in Fig. 4.2. The slope of the

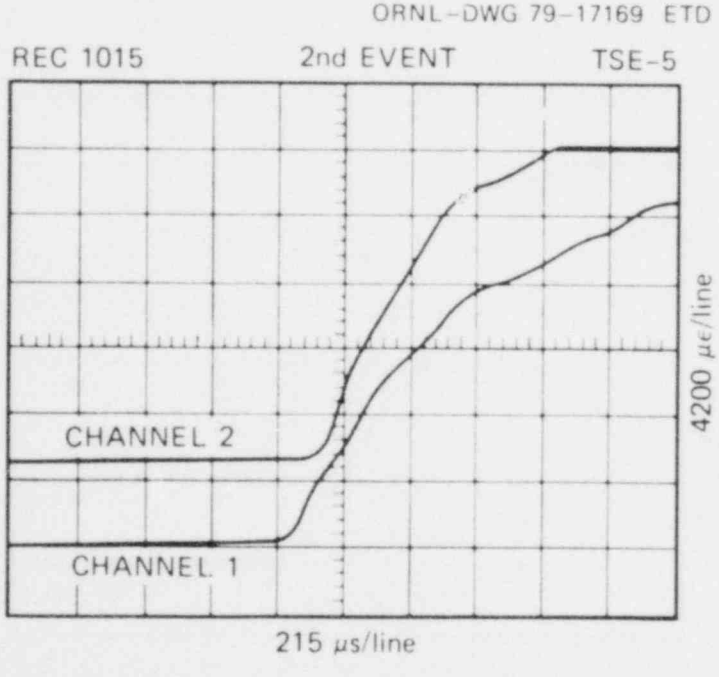

Fig. 4.2. COD output (gages 4 and 6) vs time for second crack jump during TSE-5.

steepest portion of the curve (initial straight-line segment) is

$$(6 \times 4200\ \mu\varepsilon)/(2.2 \times 215\ \mu s) = 53.2\ (\varepsilon/s)\ ,$$

and application of the COD-gage calibration factor (COD/ε = 25 mm) yielded the maximum COD rate:

$$(\dot{COD})_{max} = 53.2 \times 25 = 1.33\ m/s\ .$$

The slope of the curve of COD vs a/w in Fig. 4.1, $\Delta COD/\Delta a$, at a/w $\cong$ 0.2 is 0.0113. Thus, the estimated maximum crack velocity is

$$\dot{a}_{max} = 1.33\ (m/s)(1/0.0113) = 118\ m/s\ .$$

A velocity of 230 m/s reported previously[1] was incorrect.

4.2.3 Toughness properties of TSE-5 test cylinder material

A prolongation of the TSE-5 test cylinder (TSC-1) is being used as a source of material for characterizing TSC-1. Prior to TSE-5 an attempt was made to characterize the material, but an insufficient number of data points were obtained to define the K_{Ic} vs temperature curve properly. Furthermore, prior to TSE-5 the use of an average curve as opposed to a lower-bound curve seemed appropriate for designing the experiment, but the results of TSE-5 indicate otherwise. Thus, for proper analysis of the TSE-5 results, further characterization of the test cylinder material was necessary.

The approach this time is to test a large number of specimens at a few temperatures, rather than the other way around, in order to define more clearly the scatter in data and thus the lower-bound toughness. So far, 48 specimens (1T-CT and 2T-CT) have been tested, mostly at −18, 32, and 82°C. In addition, five K_{Ia} values have been obtained, two at 27°C and three at ~82°C. All these data, along with the K_{Ic} and K_{Ia} values deduced from TSE-5, are plotted in Fig. 4.3. Few of the data points are valid in accordance with ASTM E399, and K_{Ic} values were calculated by means of the equivalent-energy technique.

Figure 4.3 indicates that the scatter in the K_{Ic} data is ~±50%, while less scatter occurs in the much smaller sampling of K_{Ia}. The TSE-5 K_{Ia} values are about the same as those measured in the laboratory, and in

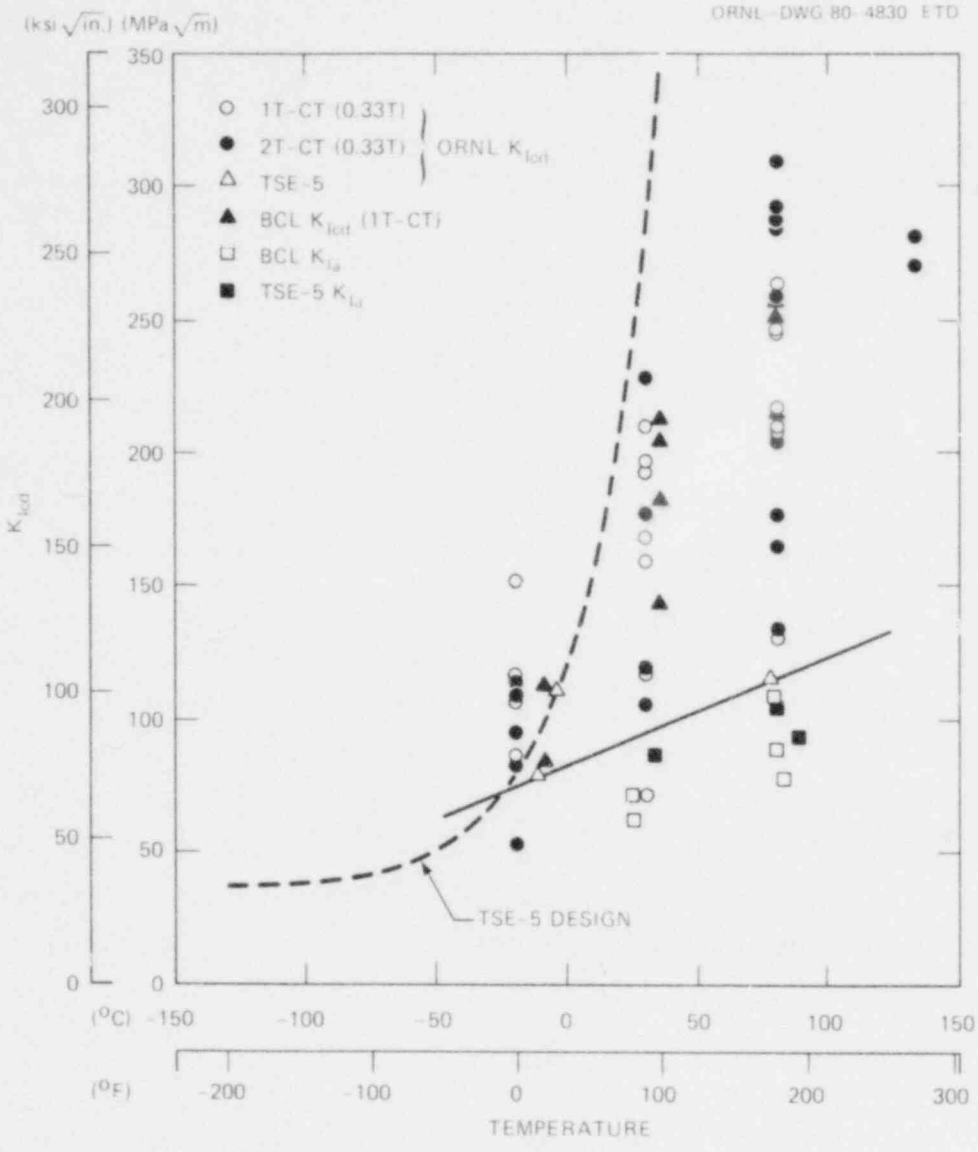

Fig. 4.3. fracture and arrest toughness values from TSE-5 and from TSC-1 prolongation.

the temperature range −20 to 40°C a curve drawn through the first and third TSE-5 K_{Ic} data points is ~28% above the lowest of the laboratory K_{Ic} values. Also, these lowest K_{Ic} values appear to coincide with the laboratory K_{Ia} values or an extrapolation thereof. At 82°C the TSE-5 curve is ~12% below the lowest laboratory K_{Ic} value. It is interesting that at 32 and 82°C the lowest of the laboratory K_{Ic} values were obtained with 1T-CT rather than the 2T-CT specimens.

The results in Fig. 4.3 indicate a trend toward lower-bound behavior on the part of the long axial flaw for the first and third initiation events during TSE-5.

4.2.4 3-D analysis of final flaw in TSE-5

As would be expected, the initial uniform-depth flaw in TSC-1 did not propagate uniformly in depth during the TSE-5 thermal transient. Because of the ability of the free ends to rotate inward, the K_I values at the ends of the cylinder tended to be smaller than elsewhere; thus less propagation occurred at the ends. Although the central portion of the cylinder, where the crack depth was reasonably uniform, seemingly could be calculated adequately with a 2-D model, a 3-D analysis was necessary as a final check on the actual crack shapes that developed during TSE-5.

Thus far the initial uniform-depth flaw and the final flaw in TSC-1 have been calculated with a 3-D model. Analysis of the initial flaw is discussed in Ref. 3, and analysis of the final flaw is discussed in the following paragraphs.

For purposes of the 3-D finite-element (FE) analysis, the final flaw shape was idealized as shown in Fig. 4.4(a); the shape was symmetrical about mid-length of the cylinder. The 3-D mesh was generated by rotating the 2-D mesh shown in Fig. 4.4(b) about the axis of the cylinder. The ADINA[4] code was used for the FE analysis, and the displacement method mentioned in Sect. 4.2.5 was used for calculating the K_I values. Details of the FE modeling and computer-related information are given in Table 4.2.

Results of the analysis are presented in Table 4.3 and Fig. 4.5. As shown in Fig. 4.5, K_I for the idealized crack front is nearly uniform along the length of the cylinder, oscillating slightly (~±7%) with a maximum near the ends. An interesting comparison is obtained by making 2-D (plane-strain) calculations for the various crack depths along the length of the cylinder. These results are also included in Table 4.3 and Fig. 4.5. For ~70% of the length of the cylinder (central portion), the 2-D and 3-D K_I results are separated by no more than 10%. Near the ends, the 2-D K_I values are considerably higher because the 2-D analysis does not include bending near the ends.

Fig. 4.4. Idealization of final arrested crack front of TSE-5 for purposes of 3-D FE analysis. (a) Partial longitudinal section through vessel wall. (b) FE model of cylinder wall used to generate 3-D mesh by rotating it about cylinder axis.

In previous 3-D studies[3,5] with uniform-depth cracks, the K_I values at midlength were about 10% higher than the corresponding 2-D plane-strain values, and near the ends the 3-D K_I values dropped sharply to zero, as shown in Fig. 4.6. These low values of K_I near the ends of the cylinder are a result of inward rotation of the ends that tends to put the crack in compression.

Table 4.2. Miscellaneous data related to 3-D FE analysis with ADINA 78 code using 1720 K bytes of fast memory

Young's modulus, GPa (ksi)	193.1 (28×10^3 ksi)
Poisson's ratio	0.3
Number of elements used to propagate mesh in circumferential direction	7
Angular dimensions of circumferential elements	1.5°, 3.5°, 10°, 30°, $3 \times 45°$
Number of nodes	3025
Number of elements	581
Number of degrees of freedom (equations)	8509
Number of matrix elements (approximate)	4.5×10^6
Maximum half bandwidth	1289
Mean half bandwidth	530
Maximum block size (real*8 words)	25,861
Number of blocks	177
IBM 3033 central processing unit time, min	37
Wall clock time, min[a]	160
Input/output thousands[b]	50
Approximate total cost, $[c]	260

[a]Can vary widely between identical runs.

[b]Depends on blocking factors.

[c]Printed output directed to microfiche.

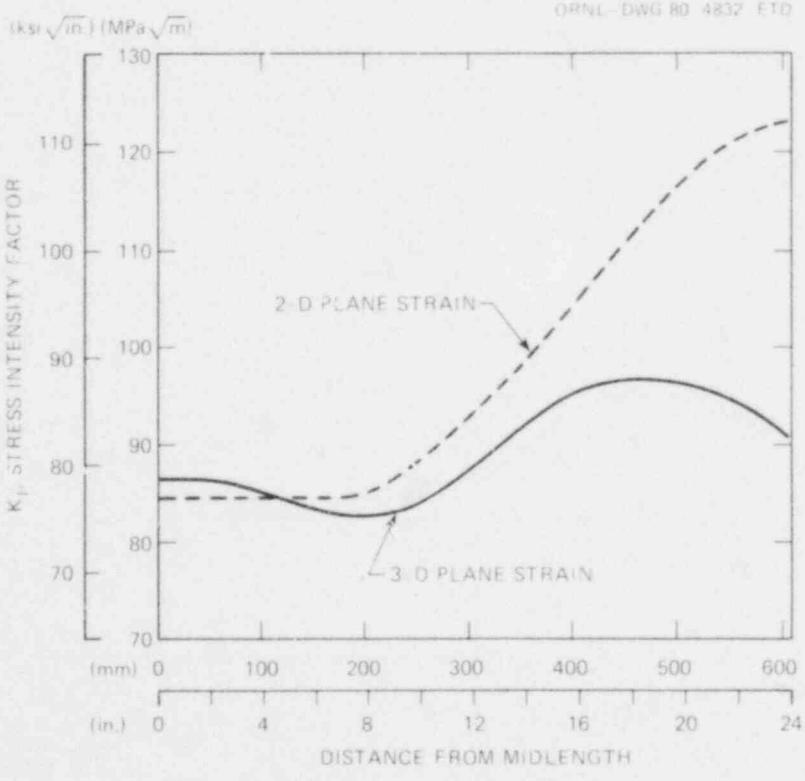

Fig. 4.5. Variation of 3-D K_I as a function of distance from midlength (solid curve). For purposes of comparison, 2-D plane-strain K_I values corresponding to fractional crack depth at each axial position are also plotted (dashed curve).

Table 4.3. CODs and stress intensity factors K_I from 2-D and 3-D FE analysis of final arrested crack shape of TSE-5

Time in transient: 3.43 min

Distance from midlength to point on crack front (mm)	Fractional crack depth (a/w)	CODs (mm)		Stress intensity factors ($MPa \cdot \sqrt{m}$)	
		3-D values[a]	2-D values	3-D values	2-D values
0	0.833	1.66	1.73	86.5	84.6
50.8	0.833	1.65	1.73	86.3	84.6
101.6	0.833	1.64	1.73	85.5	84.6
152.4	0.833	1.63	1.73	83.2	84.6
203	0.829	1.60	1.72	82.7	85.2
254	0.815	1.56	1.69	84.1	88.6
305	0.793	1.51	1.65	87.7	93.2
355	0.761	1.44	1.57	92.0	98.7
405	0.720	1.36	1.4[illegible]	95.4	104.7
455	0.670	1.26	1.36	96.7	111
505	0.612	1.14	1.21	96.0	117
554	0.544	1.01	1.06	94.5	121
605	0.468	0.86	0.88	90.9	123

[a]For points other than those opposite the flat portion, these CODs are slightly offset toward midlength. See Fig. 4.4(b).

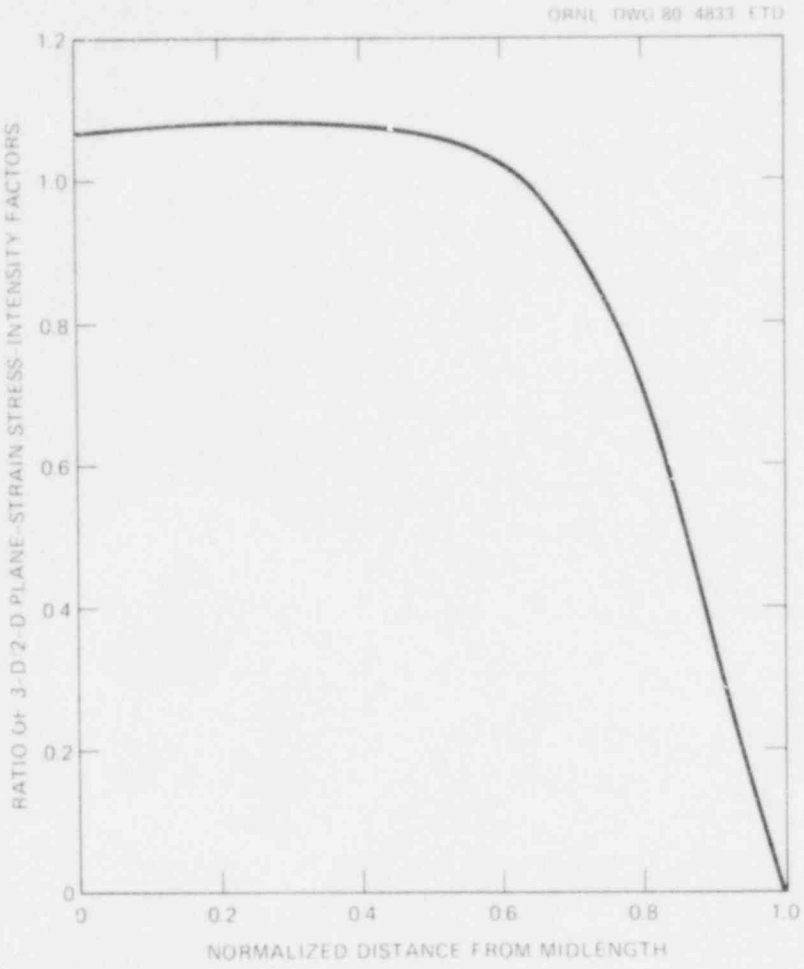

Fig. 4.6. Variation of ratio of 3-D K_I to 2-D K_I values as a function of axial distance X from midlength (normalized with respect to cylinder length 2L) for uniform crack depth of 1/2 the wall thickness.

The results of the 3-D analysis for the "actual" crack shape reflect the compensating effects of a higher K_I value for shallow cracks (2-D analysis) near the ends and a lower K_I value near the ends because of the bending effect (3-D analysis). The net result is a nearly uniform K_I value along the crack front.

The expected K_I distribution along the crack front can be determined in another manner. If the entire crack front arrests at the same instant, one can then argue that at the instant of arrest K_I/K_{Ia} is uniform along the entire crack front and equal to unity. Then, from a knowledge of K_{Ia} vs temperature and temperature vs a/w, K_I vs axial position can be obtained. Crack-tip temperatures vs axial position are shown in Fig. 4.7,

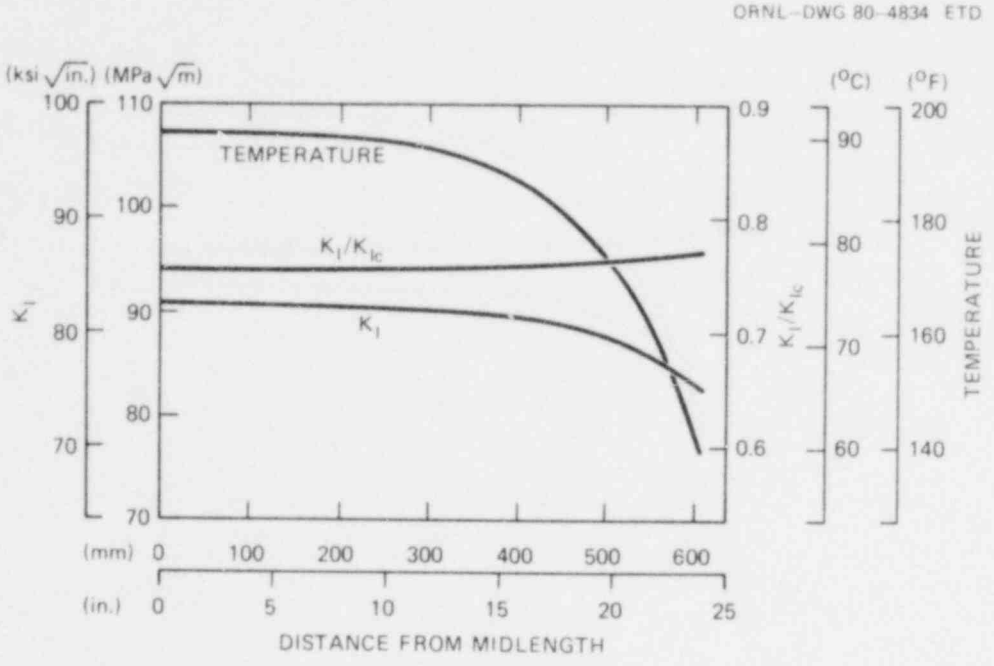

Fig. 4.7. Crack-tip temperature, K_I (deduced), and K_I/K_{Ic} as a function of axial position for TSE-5 final flaw at instant of arrest.

and a curve of K_{Ia} vs temperature can be obtained from Fig. 4.3. From these data, the K_I-vs-axial-position curve for the instant of arrest of the final crack front in TSE-5 was obtained and is presented in Fig. 4.7. A slight decrease occurs in K_I toward the end (~10% from midlength to end). This trend is more nearly realistic than that shown in Fig. 4.5 because the temperature-vs-axial position and K_{Ia}-vs-temperature trends are well established. In any case, these values do not differ greatly from the 3-D values.

It is of interest to estimate K_I/K_{Ic}-vs-axial position by means of the preceding deduced K_I distribution, the temperature distribution in Fig. 4.7, and the K_{Ic} vs temperature distribution in Fig. 4.3, even though the data do not exactly correspond to a somewhat later time in the transient when initiation might take place in the absence of warm prestressing. The resulting curve, shown in Fig. 4.7, is nearly flat, indicating that the chances of initiation are about equal along the length of the crack front. Thus, the 2-D analysis used for deducing K_{Ic} values near midlength for the shallower initiation events should be reasonably accurate.

4.2.5 Verification of calculational techniques

The results of an independent calculation of some 2-D stress intensity factors (K_I) for TSE-5 are presented to provide a check on the accuracy of the previously reported values.

The complete set of 2-D K_I values for the range of times of the TSE-5 experiment and for fractional crack depths (a/w) ranging from a/w = 0.026 through a/w = 0.90 were previously reported.[1] A check of these values by means of an independent method is desirable, and the results of such a check are presented in the following two paragraphs. The actual temperature distributions obtained during the test were used to perform the computations.

The previous results were obtained using a PE release-rate technique.[5] The PE is determined by means of the FE method using the FMECH code.[5] A second method of analysis used an 8-noded, 1/4-point element with the ADINA code[4] and the displacement method[5] to calculate K_I values. A comparison of results of the two computations is given in Table 4.4.

The difference between the results from the two methods is about 1%. Although only a small number of values has been checked, the agreement is excellent, considering that the FMECH code uses a completely different

Table 4.4. Comparison of some 2-D K_I values for TSE-5 calculated by two independent methods

Final crack arrest occurred 3.43 min into transient

Fractional crack depth (a/w)	K_I ($MPa\cdot\sqrt{m}$)	
	Potential energy release rate method	Displacement method
0.5	121.0	122.5
0.6	116.3	116.6
0.7	107.7	107.2
0.8	91.0	92.1

technique, element type, and mesh from that used in the displacement method. Moreover, the displacement method itself has been checked against the closed-form solution for the center-crack strip. The difference between the values obtained by the displacement method and those obtained by the closed-form solution is given in Fig. 4.8, which shows maximum differences of about 2%. Thus, the accuracy of the reported values for TSE-5 should be about 4%.

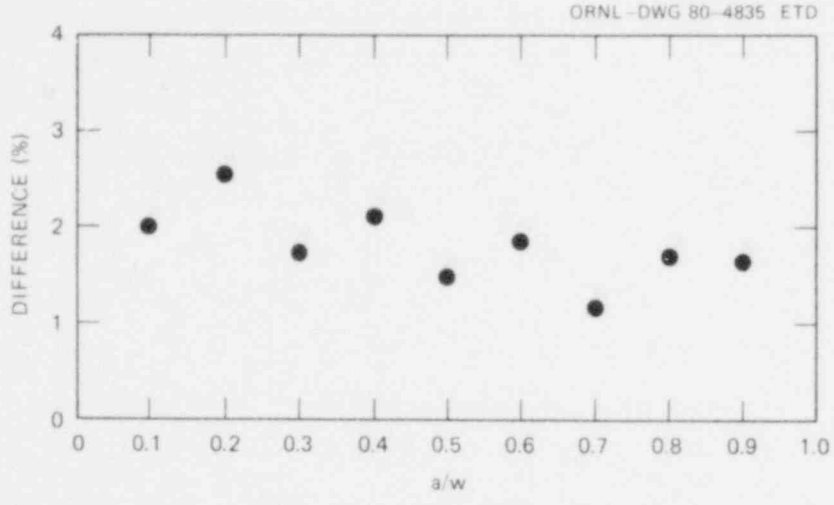

Fig. 4.8. Difference (%) between theoretical K_I values and those calculated by displacement method for a center-cracked strip as a function of fractional crack depth (a/w).

4.3 Calculations Pertaining to TSE-5A

The HSST thermal shock experiment to follow TSE-5 is intended to be the same experiment that TSE-5 was intended to be and will be designated TSE-5A. This future experiment was previously designated TSE-6.[2]

The purposes of TSE-5A are to (1) demonstrate multiple initiation-arrest events with deep penetration ($a/w \geq 0.5$), (2) demonstrate arrest in a rising K_I field [positive value of $dK_I/d(a/w)$], and (3) demonstrate warm prestressing (WPS).

As indicated in Fig. 4.3, the actual transition temperature for the TSE-5 test cylinder was much higher than specified; this prevented a demonstration of WPS or of arrest in a rising K_I field. The tempering temperature for the test cylinder material was 613°C, which was too low.

However, prior to TSE-5 higher tempering temperatures ($\bar{>}650°C$) were expected to result in lower-shelf toughness values that were too high. In preparation for TSE-5A, additional material characterization studies are being conducted for the higher tempering temperatures in hopes of finding that the lower bound of the lower-shelf toughness is actually significantly less than indicated previously.

As an alternative measure to obtaining the preferred toughness curve, TSE-5A design calculations are being made for more severe thermal shocks than specified for TSE-5. In these calculations (with two exceptions) the American Society of Mechanical Engineers (ASME) Code Sect. XI (Appendix A) K_{Ic} and K_{Ia} curves are being used, and several values of RT_{NDT} are being considered. Preliminary results of the analysis are summarized in Table 4.5. As indicated in this table, three thermal shocks were considered: (1) that specified for TSE-5, (2) that actually obtained during TSE-5 (more severe than the former), and (3) that calculated assuming the maximum heat transfer coefficient measured during previous liquid-nitrogen heat transfer experiments. The latter thermal shock is the most severe of the three and could have quenching asymmetry problems associated with it.

For judging the acceptability of a set of test conditions for TSE-5A, permissible extreme values of $(a/w)_{IWPS}$, $(a/w)_{max}$, $(K_I/K_{Ic})_{max}$, and $[(K_I/K_{Ic})_{max}]_{a/w = 0.10}$ have been established. The fractional crack depth corresponding to incipient warm prestress (IWPS) is $(a/w)_{IWPS}$, and the minimum acceptable value is ~0.30. The maximum crack depth at which arrest could take place, assuming WPS to be effective is $(a/w)_{max}$; its maximum acceptable value is 0.75, and its minimum value is $(a/w)_{IWPS}$. The maximum K ratio (with respect to time) corresponding to $(a/w)_{max}$ is $(K_I/K_{Ic})_{max}$, and its minimum acceptable value is 1.7. These first three parameters are determining factors in an adequate demonstration of WPS. The fourth and final parameter, $[(K_I/K_{Ic})_{max}]_{a/w = 0.10}$, is the maximum K ratio (with respect to time) corresponding to an initial fractional crack depth of 0.10; it is simply an indication of the potential for initiation of the initial flaw, and its acceptable minimum value is 1.5.

The first five cases in Table 4.5 correspond to the thermal shock specified for TSE-5. An RT_{NDT} somewhat less than −18°C is required to satisfy all of the previously stated conditions. An RT_{NDT} of −34°C would

Table 4.5. Fracture mechanics results from TSE-5A parametric studies

Case	K_{Ic} (source)	RT_{NDT} (°C)	$(a/w)_{IWPS}$[a]	$(a/w)_{max}$[b]	$(K_I/K_{Ic})_{max}$[c]	$[(K_I/K_{Ic})_{max}]_{a/w = 0.10}$[d]
			TSE-5 design thermal shock			
266	ASME XI	−34	0.49	0.49–0.70	2.1–1.7	2.3
257	ASME XI	−18	0.59	0.59–0.79	2.2–1.5	2.4
289	ASME XI	−1	0.70	0.70–0.86	2.0–1.3	2.4
256	Quench-only[e]		0.86	0.86–>0.86	1.2–>1.2	2.5
			TSE-5 actual thermal shock			
270	ASME XI	−34	0.44	0.44–0.62	2.6–2.1	2.8
290	ASME XI	−18	0.53	0.53–0.74	2.6–1.9	2.8
291	ASME XI	−1	0.62	0.62–0.84	2.6–1.6	2.9
271	613°C temper		0.80	0.80–>0.80	1.2–<1.2	2.9
			Maximum attainable thermal shock			
280	ASME XI	−51	0.32	0.32–0.45	2.8–2.3	3.3
279	ASME XI	−34	0.39	0.39–0.52	2.9–2.4	3.5
259	ASME XI	−18	0.43	0.43–0.59	3.0–2.4	3.6
292	ASME XI	−1	0.50	0.50–0.69	3.1–2.5	3.6

[a] Fractional crack depth corresponding to IWPS.

[b] Range of maximum crack penetration (fractional), assuming WPS to be effective.

[c] Range of $(K_I/K_{Ic})_{max}$ corresponding to range in final crack depth defined in item b above.

[d] $(K_I/K_{Ic})_{max}$ corresponding to fractional crack depth of 0.10.

[e] Heat treatment for TSE-4.

result in a very satisfactory experiment, and in effect this condition was specified for TSE-5.

Increasing the severity of the thermal shock permits a higher value of RT_{NDT}, and as shown in Table 4.5, a value of −18°C and perhaps a little higher is acceptable for the actual TSE-5 thermal shock. Increasing the severity of the shock still further to the maximum attainable permits an RT_{NDT} range of −51 to somewhat higher than −1°C. However, as mentioned previously, thermal shocks much more severe than that obtained during TSE-5 may not be acceptable because of quenching asymmetry problems.

Preliminary results from the material characterization studies indicate that the accuracy of the two previous RT_{NDT} measurements (2 and −6°C)[6] for tempering temperatures of 677 and 704°C may have uncertainties of ~±20°C, and the toughness curve corresponding to a tempering temperature of 677°C appears at this time to be shifted to the right of the TSE-5 design curve (RT_{NDT} = −34°C) by no more than ~20°C. Thus, RT_{NDT} = 18°C may be achieved, in which case the TSE-5 thermal transient will be adequate.

4.4 Thermal Shock Material Characterization

W. J. Stelzman D. A. Canonico

We have continued to characterize the fracture toughness properties of the thermal shock cylinder TSC-1 and its prolongation, TSP-1. Both the cylinder and the prolongation have received identical heat treatments, including tempers of 613°C for 4 h. We are also continuing to characterize the fracture toughness properties at higher temperatures using material from a second prolongation, TSP-2, from cylinder TSC-2 that had normalizing, austenitizing, and quenching treatments identical to those of TSC-1 and TSP-1. Two tempering temperatures (677 and 707°C) were evaluated using the TSP-2 material.

The fracture toughness results (K_{Icd}) from the TSP-1 prolongation (613°C temper) are listed in Table 4.6. Testing was conducted with CT-oriented 1T and 2T compact specimens (1TCS and 2TCS). The results in Table 4.6 and the results previously reported[7] are plotted in Fig. 4.9.

Table 4.6. Static fracture toughness (K_{Icd}) from 1T and 2T compact specimens[a] of quenched prolongations TSP-1 and TSP-2 after tempering at 613, 677, and 707°C

Temperature (°C)		Static fracture toughness K_{Icd} ($MN \cdot m^{-3/2}$)	Temperature (°C)		Static fracture toughness K_{Icd} ($MN \cdot m^{-3/2}$)
Temper[b]	Test		Temper[b]	Test	
613	−18	106	677	−4	237
		151			211
		116			
		86		24	235
		108[c]			261
		94[c]			295
		53[c]			304
		114[c]			245
		83[c]			267
					282
	32	117			164
		193			
		160	707	−46	153
		196			143
		168			163
		209			167
		71			171
		228[c]			91
		118[c]			136
		106[c]			138
		176[c]			158
					157
	82	244			157
		208			
		262		−4	367
		246			155
		217			
		204[c]		38	312
		165[c]			372
		284[c]			244
		288[c]			345
		310[c]			337
		294[c]			382
					342
	135	281[c]			347
677	−4	118			402
		254		66	317

[a]CT-oriented.

[b]Tempered for 4 h, air-cooled.

[c]2T compact specimens; remainder 1T.

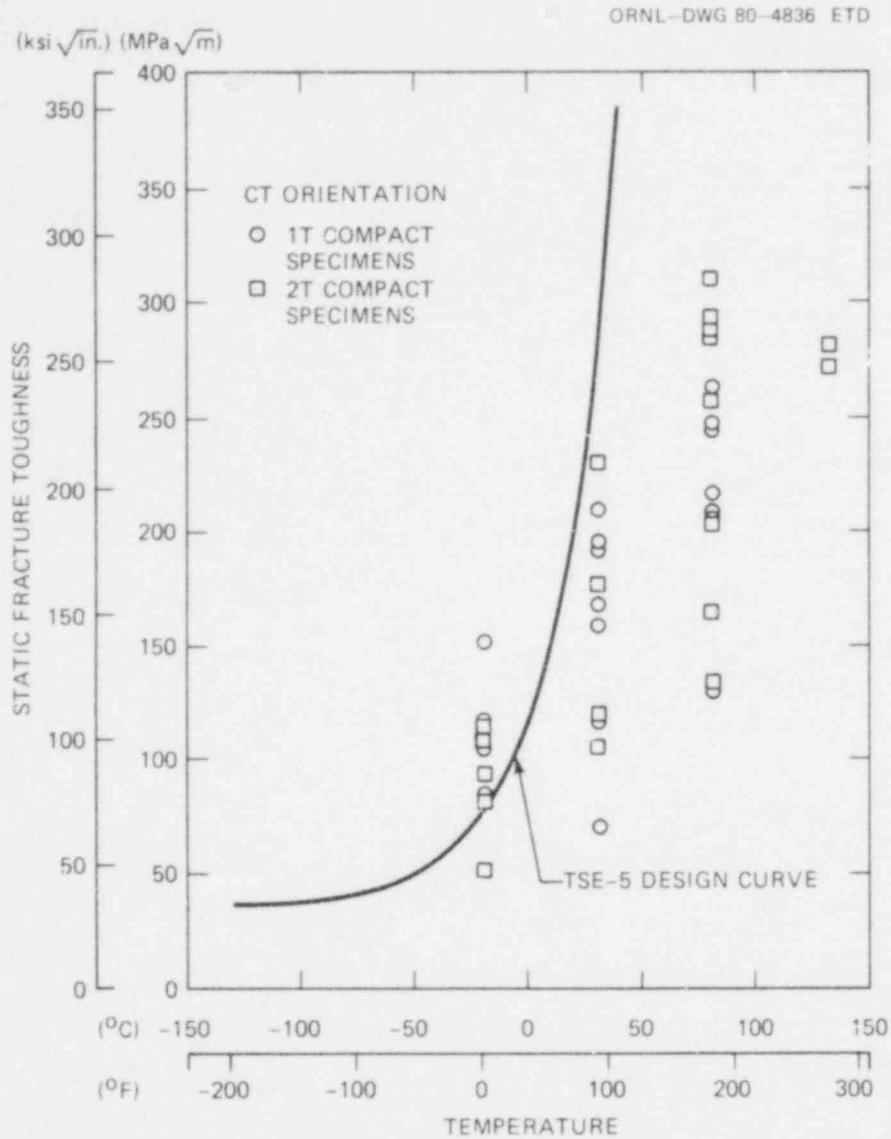

Fig. 4.9. Variation of static fracture toughness (K_{Icd}) from 1T and 2T compact specimens taken from prolongation TSP-1 (SA 508) after tempering at 613°C for 4 h and cooling in air.

Three 2TCS tests were valid according to the American National Standards Institute/American Society for Testing and Materials (ANSI/ASTM) E 399-78 standard at −18°C. These specimens had K_{Ic} values of 53, 83, and 94 $MN \cdot m^{-3/2}$. The results show that in the transition temperature regime the K_{Icd} values vary over a considerable range with the possibility that the lowest K_{Icd} value obtained during testing may not be the lowest value attainable. Differences in K_{Icd} values ranging as high as 137 $MN \cdot m^{-3/2}$ and

176 $MN \cdot m^{-3/2}$ were obtained using 1TCS and 2TCS respectively. Additional testing is contemplated for the 613°C temper using 2TCS.

The K_{Icd} results from prolongation TSP-2 tempered at 677 and 707°C were also obtained with CT-oriented 1TCS. The results are also listed in Table 4.6 and plotted in Figs. 4.10 and 4.11 together with the results previously reported.[7] Figure 4.10 also includes the results obtained by

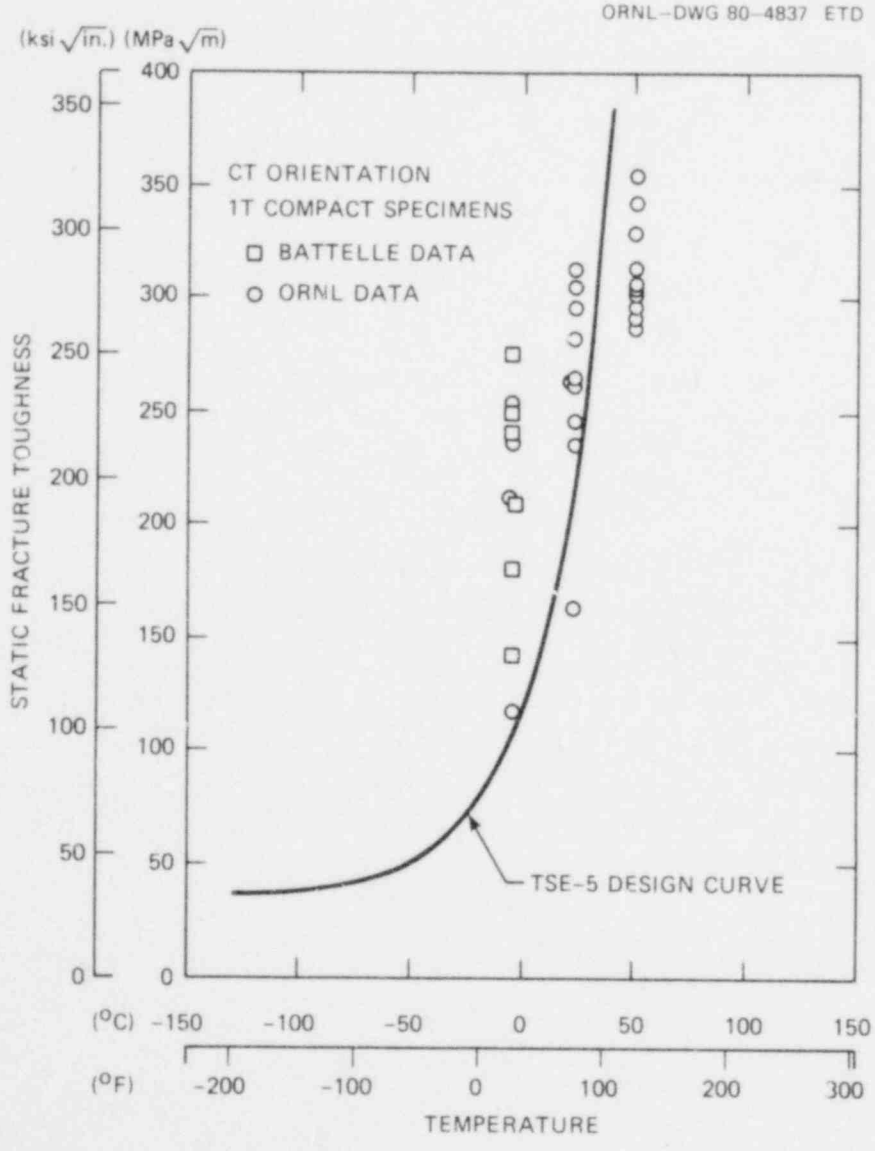

Fig. 4.10. Variation of static fracture toughness (K_{Icd}) from 1T compact specimens taken from prolongation TSP-2 (SA 508) after tempering at 677°C for 4 h and cooling in air.

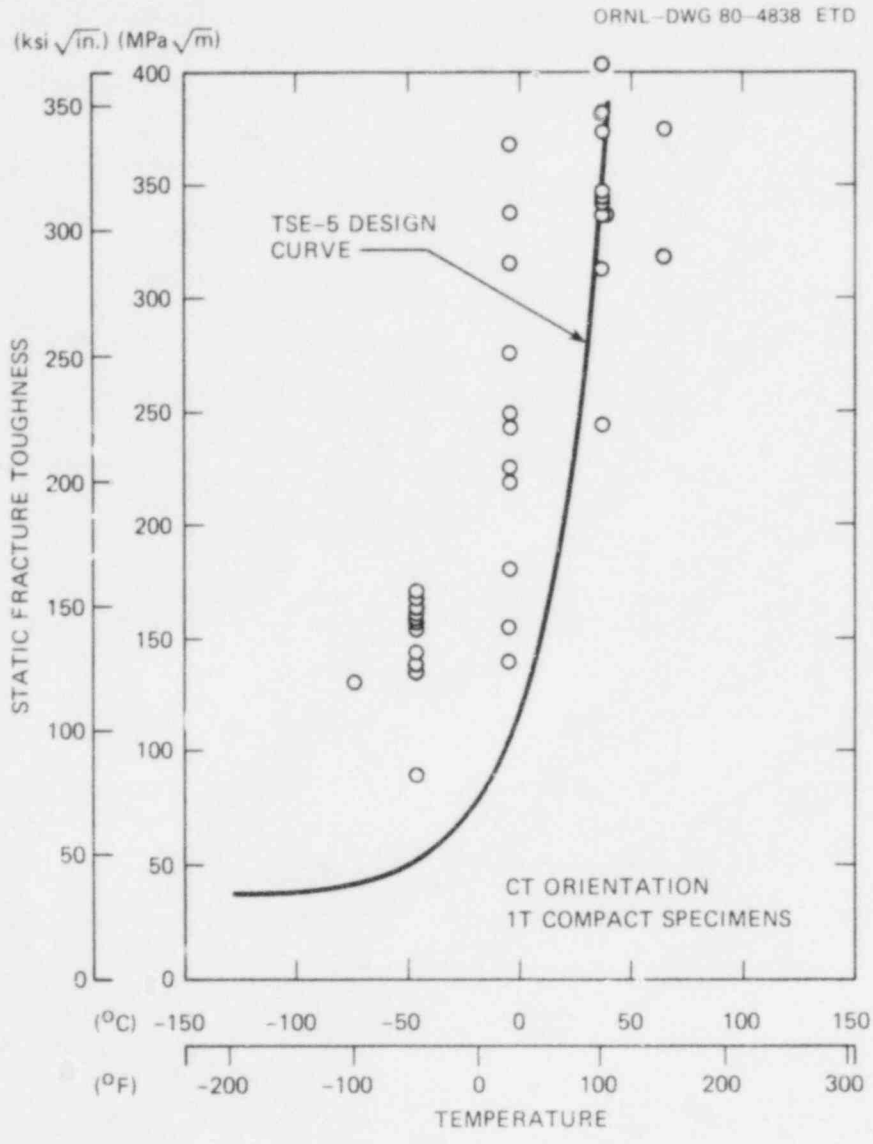

Fig. 4.11. Variation of static fracture toughness (K_{Icd}) from 1T compact specimens taken from prolongation TSP-2 (SA 508) after tempering at 707°C for 4 h and cooling in air.

the Battelle Memorial Institute[8] with TSP-2 material tempered at 677°C. The values agree with the results obtained at ORNL. Variations in K_{Icd} values were as high as 154 $MN \cdot m^{-3/2}$ for the 677°C tempered material and 220 $MN \cdot m^{-3/2}$ for the 707°C tempered material.

References

1. R. D. Cheverton, S. E. Bolt, and P. P. Holz, "Thermal Shock Investigations," *Heavy-Section Steel Technology Program Quart. Prog. Rep. July–September 1979*, NUREG/CR-1197 (ORNL/NUREG/TM-370), pp. 52–80.

2. R. D. Cheverton, S. E. Bolt, and S. K. Iskander, "Thermal Shock Investigations," *Heavy-Section Steel Technology Program Quart. Prog. Rep. October–December 1979*, NUREG/CR-1305 (ORNL/NUREG/TM-380), pp. 62–88.

3. R. D. Cheverton, "Thermal Shock Investigations," *Heavy-Section Steel Technology Program Quart. Prog. Rep. July–September 1978*, NUREG/CR-0476 (ORNL/NUREG/TM-275), pp. 61–89.

4. Klaus-Jurgen Bathe, *ADINA — A Finite Element Program for Automatic Dynamic Incremental Nonlinear Analysis*, Report 82448-1, Acoustics and Vibration Laboratory, Mechanical Engineering Department, Massachusetts Institute of Technology, Cambridge, MA (September 1975; rev. December 1978).

5. S. K. Iskander, *Two Finite Element Techniques for Computing Model I Stress Intensity Factors in Two- and Three-Dimensions Problems*, ORNL/NUREG/CSD/TM-14 (1980).

6. W. J. Stelzman and D. A. Canonico, "Thermal Shock–Temper Study," *Heavy-Section Steel Technology Program Quart. Prog. Rep. January–March 1979*, NUREG/CR-0818 (ORNL/NUREG/TM-324), pp. 104–11.

7. W. J. Stelzman and D. A. Canonico, "Thermal Shock Material Characterization," *Heavy-Section Steel Technology Program Quart. Prog. Rep. October–December 1979*, NUREG/CR-1305 (ORNL/NUREG/TM-380), pp. 81–87.

8. A. R. Rosenfield, Battelle Memorial Institute, private communication to R. D. Cheverton, Oak Ridge National Laboratory, Feb. 13, 1980.

5. PRESSURE VESSEL INVESTIGATIONS*

5.1 Intermediate Test Vessel V-8A

P. P. Holz

5.1.1 Test objectives

The results from nuclear reactor test and irradiation surveillance programs indicate that the Charpy V-notch upper-shelf energies (USE) of some beltline-region welds of reactor vessels could, during their lifetime, decrease below 68 J, which is the level for adjusting the reference temperature for irradiation effects. Intermediate test vessel V-8 of the HSST program is to be seam-welded with low-USE (47.5- to 74.6-J) weld metal to provide a flaw site for vessel test V-8A, in which crack extension in this weld metal will be studied at upper-shelf conditions. The results will be compared with fracture mechanics analyses based on data obtained from fracture toughness and J integral specimens. The low-USE longitudinal vessel seam and weld test specimens will be prepared so that they will be similar to the reactor vessel beltline-region welds prior to irradiation, except that they will have lower USE.

Since irradiated metal submicrostructure cannot be achieved by methods not involving high energy particle irradiation, lower-than-normal USE must be achieved by some other means, such as by chemical composition and by microstructure control. Thus, simulation of the irradiated metal in the V-8A test is limited to control of the macroscopic material properties, the 47.5- to 74.6-J USE and 450- to 620-MPa yield strength (YS) values. The fracture toughness and crack-growth resistance properties of the unirradiated low-USE weld metal will also be evaluated and compared with those of irradiated weld metal before further confidence can be placed in the accuracy of this simulation.

Another objective of the HSST program is testing low-USE weld metal regardless of irradiation damage to evaluate the usefulness of small-

---

*Conversions from SI to English units for all SI quantities are listed on a foldout page at the end of this report.

specimen test results and fracture mechanics analysis in predicting pressure vessel material behavior.

5.1.2 Welding process development and demonstration

A subcontract purchase order is being awarded to the Babcock and Wilcox (B&W) Company, Alliance Research Center, Alliance, Ohio, to (1) develop a special welding process for the low-USE seam weld, (2) prepare vessel V-8A and characterization weldments by this process, and (3) perform material characterization tests. This work is divided into seven tasks, which will be performed in three phases. Phase I includes Tasks 1 and 2: Task 1 consists of research and development trials to develop and demonstrate the special welding process;[1] under Task 2, B&W will also prepare quality assurance plans, shop drawings, and specifications incorporating the procedures developed under Task 1 for the vessel V-8 seam and repair welds. All results of the test examinations from Task 1 trial welds will be reported to the HSST project under Task 2. The HSST project has the right to terminate the subcontract at the completion of Phase I if the desired weld metal properties are not achieved.

5.1.3 Characterization and vessel welds

Phase II work includes Task 3, making the characterization welds; Task 4, vessel V-8 welds; and Task 5, a weldment for our use for practice flawing.

Phase III consists of Tasks 6 and 7. Task 6 involves machining specimens from the characterization weldment, testing specimens, and reporting data; and Task 7 comprises preparation and issuance of a final detailed documentary report giving a chronological description of all fabrication work performed. The report is also to include a compilation of all data obtained in chemical, mechanical, and metallurgical specimen testing.

5.2 Proposed Acoustic Emission Tests

Discussions continued with researchers at Pacific Northwest Laboratories (PNL) in regard to making appropriate repairs to intermediate test

vessel V-7 and preparing fatigue-sharpened flaws to ready the vessel for a series of tests (V-7AE) in which acoustic emission (AE) would be observed during cyclic loading.[2]

Tests with vessel V-7 would be at ambient to 93°C vessel temperatures with graphite filler blocks placed in the vessel void to maximize cycling frequency. An internal concentric dip tube could also be installed through the vessel head to incorporate a source of fluid flow noise, which was a desired environmental test condition. Vessel V-7AE would include three inside surface flaws placed in its midsection. Two of the interior flaws would be presharpened; the other would consist of a machined notch only. Stainless steel weld-overlay cladding would be added to an area of ~0.1 m^2 on the inside surface of the vessel. Inclusions in weld metal could be added to a repair weld of a partial penetration hole to provide a source of AE not associated with a sharp flaw.

Relief for postweld stress of the plug-weld repair of the existing cavity in test vessel V-7 was recommended to eliminate residual stresses. Cost analyses for vessel repair and test preparation indicate that machining and fatigue-sharpening inside-surface flaws in plugs that would subsequently be welded into the vessel would be less costly than preparing the flaws in place.

As an alternative to using vessel V-7, preparation of flawed plugs that would be welded into a German test vessel was considered. Cost estimates were made for options in which PNL or NRC expressed interest.

References

1. P. P. Holz, "Intermediate Vessel Test V-8A," *Heavy-Section Steel Technology Program Quart. Prog. Rep. October–December 1979*, ORNL/NUREG/TM-380, pp. 89–90.

2. R. H. Bryan, "Proposed AE Tests with Vessel V-7 (V-7AE)," *Heavy-Section Steel Technology Program Quart. Prog. Rep. October–December 1979*, ORNL/NUREG/TM-380, pp. 90–92.

CONVERSION FACTORS[a]

SI unit	English unit	Factor
mm	in.	0.0393701
cm	in.	0.393701
m	ft	3.28084
m/s	ft/s	3.28084
kN	lb_f	224.809
kPa	psi	0.145038
MPa	ksi	0.145038
$MN \cdot m^{-3/2}$ ($MPa \cdot \sqrt{m}$)	ksi $\sqrt{in.}$	0.910048
J	ft-lb	0.737562
k	°F or °R	1.8
KJ/m^2	$in.-lb/in.^2$	5.71015
$W \cdot m^{-2}\ K^{-1}$	Btu/h-ft^2-°F	0.176110
$T(°F) = 1.8\ T(°C) + 32$		

[a]Multiply SI quantity by given factor to obtain English quantity.

NUREG/CR-1477
ORNL/NUREG/TM-393
Dist. Category RF

Internal Distribution

1. R. G. Berggren
2. S. E. Bolt
3-7. R. H. Bryan
8. J. W. Bryson
9. D. A. Canonico
10. R. D. Cheverton
11. J. M. Corum
12. W. R. Corwin
13. W. P. Cottrell
14. W. L. Greenstreet
15. R. C. Gwaltney
16. P. P. Holz
17. S. K. Iskander
18. K. K. Klindt
19. J. G. Merkle
20. C. A. Mills
21. S. E. Moore
22. F. R. Mynatt
23. D. J. Naus
24. F. H. Neill
25. J. L. Rich
26. C. C. Robinson
27. G. M. Slaughter
28. J. E. Smith
29. W. J. Stelzman
30. H. E. Trammell
31-35. G. D. Whitman
36. Patent Office
37. Central Research Library
38. Document Reference Section
39-40. Laboratory Records Department
41. Laboratory Records (RC)

External Distribution

42. C. Z. Serpan, Reactor Safety Research, Nuclear Regulatory Commission, Washington, DC 20555
43. M. Vagins, Reactor Safety Research, Nuclear Regulatory Commission, Washington, DC 20555
44. Office of Assistant Manager for Energy Research and Development, DOE, ORO, Oak Ridge, TN 37830
45-46. Technical Information Center, DOE
47-476. Given distribution as shown in category RF (NTIS — 10)

☆ U.S. GOVERNMENT PRINTING OFFICE: 1980-640-245/153